1 Results: ΛK^0_S and $\Lambda K^{\pm}$ (Additional Figures)

This appendix presents fit results obtained using different methods and variations of our fit procedure. The purpose here is to offer a more in depth and transparent look at how the various assumptions made for our final fit procedure affect our results. For all cases, the interesting result remains of the ΛK^+ system exhibiting a negative $\Re f_0$, the ΛK^- positive, and the ΛK^0_S system somewhere between.

For our final results, we have chosen to include three residual contributors, as this best matches the experimental situation. These three contributors include: (Σ^0K, Ξ^0K, Ξ^-K) $\rightarrow \Lambda$K. Moving to ten contributors, we additionally include feed-down from ($\Sigma^{*(+,-,0)}K^{*0}$, ΛK^{*0}, $\Sigma^0 K^{*0}$, $\Xi^0 K^{*0}$, $\Xi^- K^{*0}$) $\rightarrow \Lambda$K. As stated in Sec. **??**, femtoscopic analyses are sensitive to the pair emission structure at kinetic freeze-out, therefore any particle born from a resonance decaying before last rescattering is seen as primary. The Σ^* and K^* resonances have proper decay lengths $c\tau \approx 5$ fm and 4 fm, respectively. Although some of these will decay after, we expect that most will decay before kinetic freeze-out. Therefore, it is best to treat Λ and K particles originating from these resonances as primary, and therefore include only three residual contributors in our fit procedure. However, it is still interesting to observe how these additional sources of residuals would affect our fit results, as the actual situation lies somewhere between the two cases (although, weighted much more towards the three residuals case). For a more precise treatment (not warranted here, when considering all of the approximations in the measurement), one should estimate the number of Σ^* and K^* resonances decaying after kinetic freeze-out, and use this information to adjust the λ parameters.

In Appendix 1.1 we present summary plots demonstrating the effect on the extracted fit parameter sets of utilizing the different fit techniques. The comparisons include the effect of using different numbers of residual contributors, fixing the overall λ_{Fit} parameter compared to allowing it to be free, fitting a correlation function built with the Stavinskiy method compared to the normal construction method, sharing radii among all ΛK systems compared to sharing radii between only the $\Lambda K^{\pm}$ systems, and using the experimental $\Xi^- K^{\pm}$ data compared to modeling it with a Coulomb-only curve for use in the residuals treatment.

The final three subsections include a more thorough look into utilizing three (App. 1.2), ten (App. 1.3), and no (App. 1.4) residual contributors in the fit routine. These subsections match closely the structure of Sec. **??**, where we presented the final results for our ΛK study. Each begins with a summary plot compactly showing the extracted fit parameters, and each contains figures showing the fit plotted on top of the experimental data. Different from Sec. **??**, the correlations are shown out to ~ 1 GeV/c (instead of ~ 0.3 GeV/c), to show both the signal region and the non-femtoscopic background. Furthermore, Appendices 1.2 and 1.3 contain figures showing the final fit with the components describing the different residual contributions, on top of the experimental data.

As with the results presented in Sec. **??**, unless otherwise noted, the following hold true: All correlation functions were normalized in the range $0.32 < k^* < 0.40$ GeV/c, and fit in the range $0.0 < k^* < 0.30$ GeV/c. For the ΛK^- and $\bar{\Lambda} K^+$ analyses, the region $0.19 < k^* < 0.23$ GeV/c was excluded from the fit to exclude the bump caused by the Ω^- resonance. The non-femtoscopic backgrounds for the ΛK^+ and ΛK^- systems were modeled by a (6^{th}-)order polynomial fit to THERMINATOR simulation, while those for the ΛK^0_S were fit with a simple linear form. All analyses were fit simultaneously across all centralities, with a single radius and normalization λ_{Fit} parameter for each centrality bin. Scattering parameters ($\Re f_0$, $\Im f_0$, d_0) were shared between pair-conjugate systems, but assumed unique between the different ΛK charge combinations (i.e. a parameter set describing the ΛK^+ & $\bar{\Lambda} K^-$ system, a second set describing the ΛK^- & $\bar{\Lambda} K^+$ system, and a third for the ΛK^0_S & $\bar{\Lambda} K^0_S$ system). Each correlation function received a unique normalization parameter. The fits were corrected for finite momentum resolution effects, non-femtoscopic backgrounds, and residual correlations resulting from the feed-down from resonances. Lines and boxes on the experimental data represent statistical and systematic errors, respectively.

In the figures showing experimental correlation functions with fits, the black solid curve represents the primary (ΛK) correlation's contribution to the fit. The green line shows the fit to the non-flat background. The purple points show the fit after all residual contributions have been included, and momentum resolution and non-flat background corrections have been applied. The extracted fit values with uncertainties are printed as (fit value) $\pm$ (statistical uncertainty) $\pm$ (systematic uncertainty).

1.1 Fit Method Comparisons

The figures in this appendix show comparisons of extracted fit parameters obtained using different fit techniques. Fig. 1 shows a comparison of results obtained using three, ten, and no residual contributors. In Fig. 2, we demonstrate the effect of fixing the overall λ_{Fit} parameter compared to allowing it to be free (see Eq. **??** in Sec. **??**). Fig. 3 compares our normal fit results to those obtained when the correlation functions are built using the Stavinskiy method (see Sec. **??**). Fig. 4 shows the difference between sharing radii among all ΛK systems versus only sharing radii between the $\Lambda K^{\pm}$ systems. Finally, Fig. 5 shows the effect of using the experimental $\Xi^{-}K^{\pm}$ data compared to modeling it with a Coulomb-only curve for use in the residuals treatment (see Sec. **??**).

All of the figures follow the same four-panel structure: [Top Left]: $\Im f_0$ vs. $\Re f_0$, together with d_0 to the right. [Top Right (Bottom Left, Bottom Right)]: λ vs. Radius for the 0-10% (10-30%, 30-50%) bin. The ΛK^{+} system is always presented with red markers, the ΛK^{-} with blue, and the ΛK^{0}_{S} with black. In the case of all ΛK analyses sharing radii, the markers are gold. In the case of only the $\Lambda K^{\pm}$ analyses sharing radii, the markers are magenta. The square symbols in the first column of the legends are to signify the color scheme. The black symbols in the second column of the legend describe the fit procedure used.

To better explain the description in the legends, take Fig. 1 as an example. The square symbols in the first column of the top left figure indicate that the ΛK^{+} scattering parameters are shown in red, the ΛK^{-} in blue, and the ΛK^{0}_{S} in black. The symbols in the second column of the top left figure indicate that the case of three residual contributors is shown with closed circles, ten residual contributors with open crosses, and no residuals with open triangles. For the λ vs. radii plots, the square symbol describing the color scheme in the first column of the top right figure shows that all ΛK analyses share common radii and are shown with gold markers.

Fig. 4 is a bit more involved example, in terms of the markers, so it is worthwhile to explain as a second example. The square symbols in the first column of the top left figure indicate that the ΛK^{+} scattering parameters are shown in red, the ΛK^{-} in blue, and the ΛK^{0}_{S} in black. The symbols in the second column of the top left figure indicate that the case where all ΛK analyses share common radii is shown with closed circles, the case of only $\Lambda K^{\pm}$ analyses sharing radii is shown with open crosses, and the ΛK^{0}_{S} system being fit alone is shown with open triangles. For the λ vs. radii plots, the square symbols describing the color scheme in the first column of the top right figure show that the case where all ΛK analyses share common radii is drawn with gold (in addition to being closed circles, as just described) markers, only $\Lambda K^{\pm}$ analyses sharing radii is shown with magenta (in addition to open crosses, as just described) markers, and the ΛK^{0}_{S} system being fit alone is shown with black (in addition to open triangles, as just described) markers.

Fig. 1 shows a comparison of results obtained using three, ten, and no residual contributors. A more detailed look of the fit with the experimental data can be found in Appendices 1.2 - 1.4. As shown, the scattering parameters vary significantly between the different cases. For the case of no residual contributors, we would expect the λ_{Fit} parameters to be closer to $\lambda_{\text{Fit}} \sim 0.5$, when considering the value extracted for primary pairs using simulation in Table **??**. For the case of 10 residual contributors, the figure shows the magnitude of the scattering parameters tends to increase, as do the λ_{Fit} parameters. The improper treatment of the residuals places less emphasis on the primary interaction, as conveyed through the relative strength of the λ_{Fit} parameters between the three and ten residuals case, presented in Tab. **??**. More emphasis is placed on the residual contributors, whose signal is effectively flattened after being run

through the appropriate transform matrices (as shown in Figs. **??** and **??** of Sec. **??**). This leads to a lot of mostly flat contributions, as shown e.g. in Fig. 17 in App. 1.3. These two effects could account for the (mostly) larger in magnitude scattering parameters and $\lambda_{\rm Fit}$ parameters extracted when assuming 10 residual contributors.

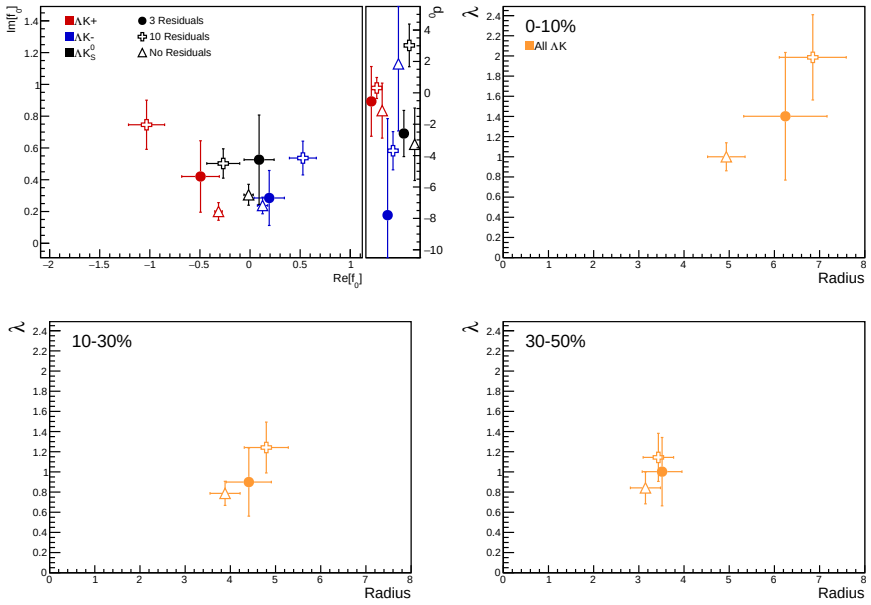

Fig. 1: Results shown for the case of 3 (closer, circles), 10 (open, crosses), and no (open, triangles) residual contributors included in the fit. See text at beginning of section for color scheme information.

In Fig. 2 we demonstrate the effect of fixing the overall $\lambda_{\rm Fit}$ parameter compared to allowing it to be free (see Eq. **??** in Sec. **??**). As shown, the extracted scattering parameters are mostly unaffected by this choice. The radii behave as expected, when considering the $\lambda_{\rm Fit}$ and R parameters are strongly correlated. For instance, forcing $\lambda_{\rm Fit}$ to decrease, as in the 0-10% centrality bin shown in the top right of the figure, causes the fit radius to also decrease.

Fig. 3 compares our normal fit results to those obtained when the correlation functions are built using the Stavinskiy method (see Sec. **??**). As shown in the figure, with the exception of the d_0 parameters (which are difficult for us to resolve experimentally), the results from the two methods are within errors of each other. As implemented in this analysis, the Stavinskiy method does a good job of reducing the non-femtoscopic background, but does not completely eliminate it. Nonetheless, it is a simple and elegant method, and should be investigated further in the future.

Fig. 4 shows the different between sharing radii among all ΛK systems versus only sharing radii between the $\Lambda K^{\pm}$ systems. As shown in the figure, the $\Lambda K^{\pm}$ systems give consistent results whether or not the ΛK^0_S system is included in the fit. The ΛK^0_S system, however, gives significantly different results when fit by itself. The ΛK^0_S system suffers the most from low statistics, and is the most difficult to fit (for instance, when fit by itself, the $\lambda_{\rm Fit}$ parameter has to be limited between [0.6, 1.1] to give realistic results). As shown, when fit alone, the ΛK^0_S fit settles on much smaller radii compared to the $\Lambda K^{\pm}$ systems. As we expect the ΛK^0_S system to share similar radii with the $\Lambda K^{\pm}$ systems, we chose to join the three together to combat the low statistics available to the ΛK^0_S. The purpose of this figure is mainly to demonstrate how the inclusion of the ΛK^0_S affects the $\Lambda K^{\pm}$ results, not the other way around.

Finally, Fig. 5 shows the effect of using the experimental $\Xi^- K^{\pm}$ data compared to modeling it with a Coulomb-only curve for use in the residuals treatment (see Sec. **??**). As shown, the results are consistent. The use of a the experimental data is preferable in that no assumption need to be made about the parent

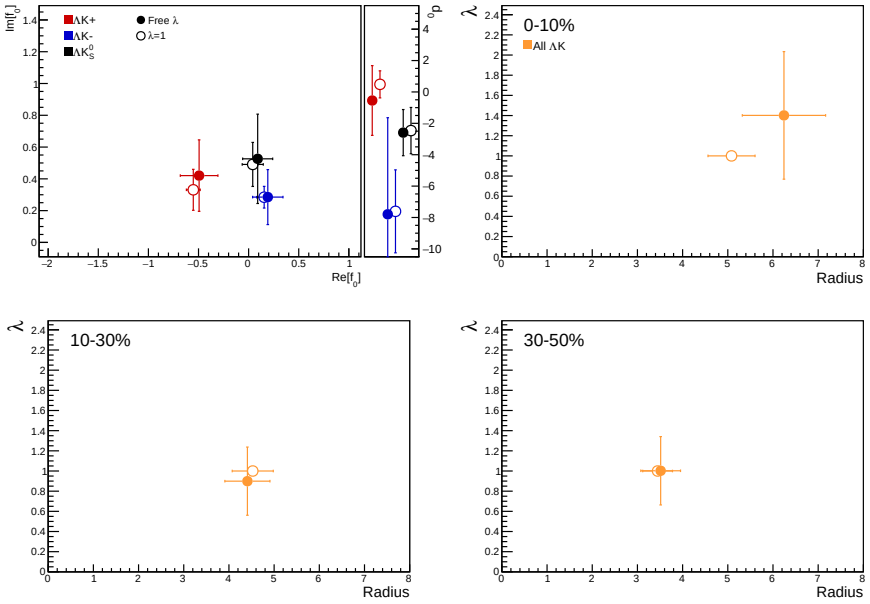

Fig. 2: Results shown for λ_{Fit} parameters left free (closed, circles) and fixed to 1 (open, circles). See text at beginning of section for color scheme information and Eq. **??** in Sec. **??** for more information on the λ_{Fit} parameter.

system's correlation function. However, the low statistics of the parent $\Xi^{-}\text{K}^{\pm}$ data (especially in the 30-50% centrality bin) could be reason to instead use the Coulomb-only curve. In our description, we choose to use the experimental data, although, as shown in the figure, the choice does not matter much.

1.2 3 Residual Contributors Included in Fit

This section presents our final results, for which three residual contributors were assumed. These three contributors include: $(\Sigma^{0}\text{K}, \Xi^{0}\text{K}, \Xi^{-}\text{K}) \rightarrow \Lambda\text{K}$. The figures presented do contain supplemental information to that presented in Sec. **??**, but are here largely for convenience in comparing to the cases of including 10 (App. 1.3) and no (App. 1.4) residual contributors.

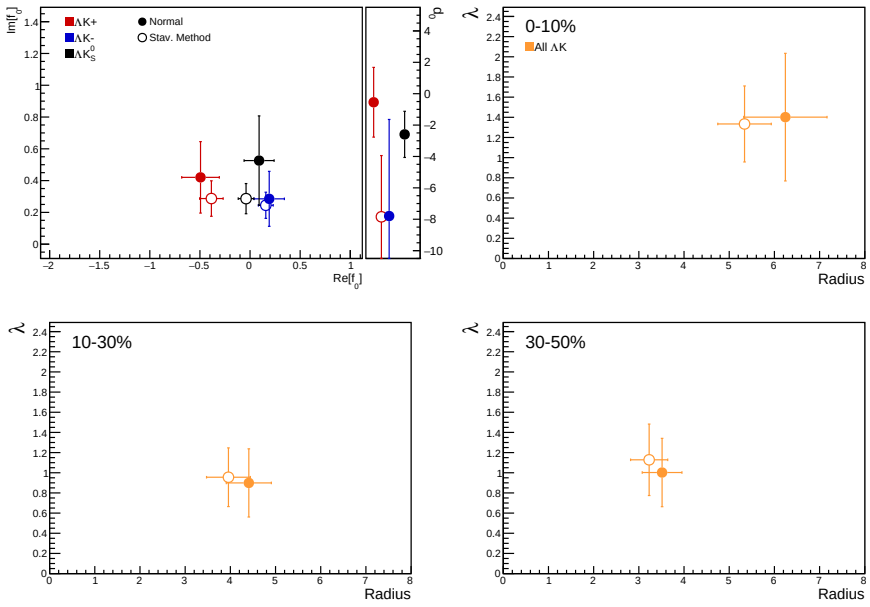

Fig. 3: Results shown for normal correlation function construction (closed, circles) and when built using the Stavinskiy method (open, circles). See text at beginning of section for color scheme information and Sec. **??** for more information on the Stavinskiy method.

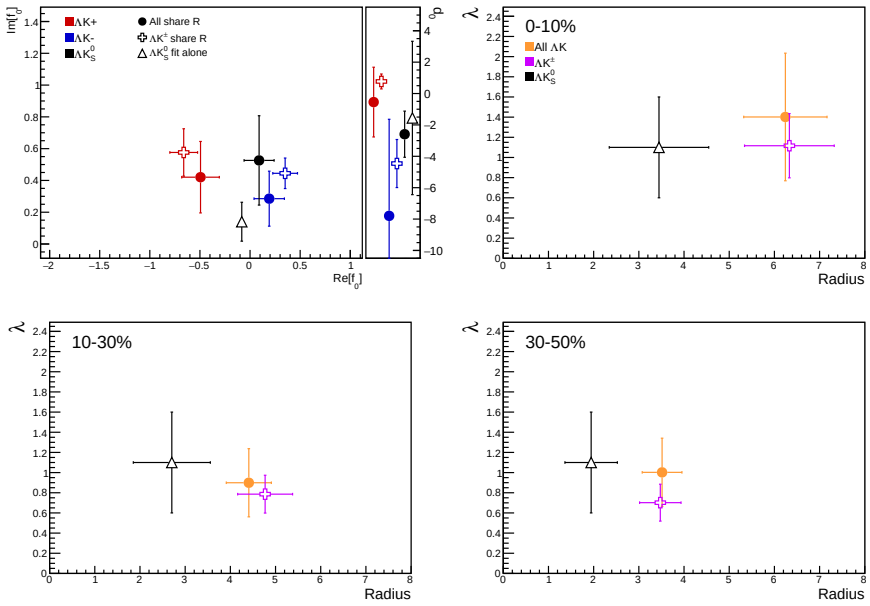

Fig. 4: Results shown for the case of all ΛK analyses sharing radii (closed, circles) and only the $\Lambda K^{\pm}$ analyses sharing radii (open, crossed), with the ΛK^0_S system fit separately (open, triangles). See text at beginning of section for color scheme information.

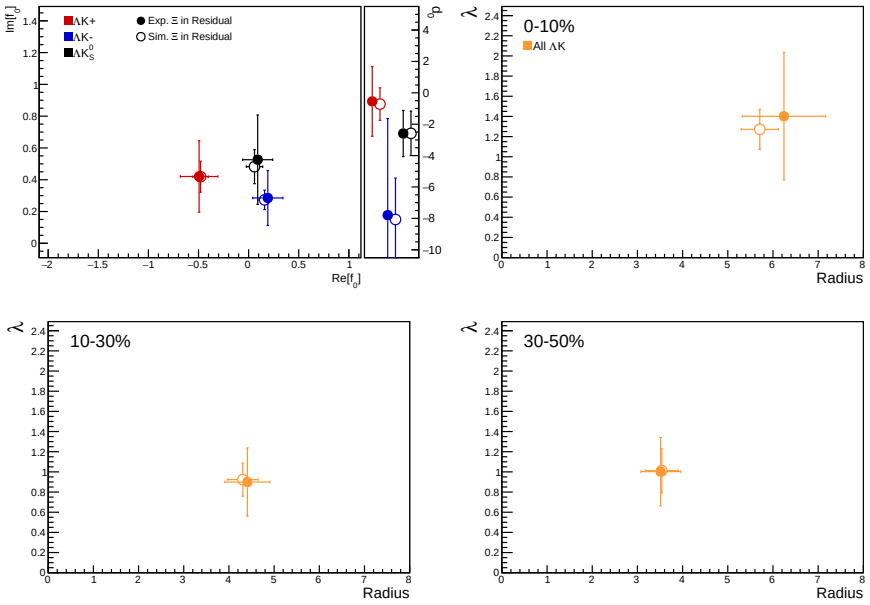

Fig. 5: Results shown when using experimental $\Xi^-\mathrm{K}^\pm$ data (closed, circles) and when simulating the $\Xi^-\mathrm{K}^\pm$ correlation function with a Coulomb-only curve (open, circles) for use in the treatment of the residual. See text at beginning of section for color scheme information, and Sec. **??** for more information on the $\Xi^-\mathrm{K}^\pm$ simulation.

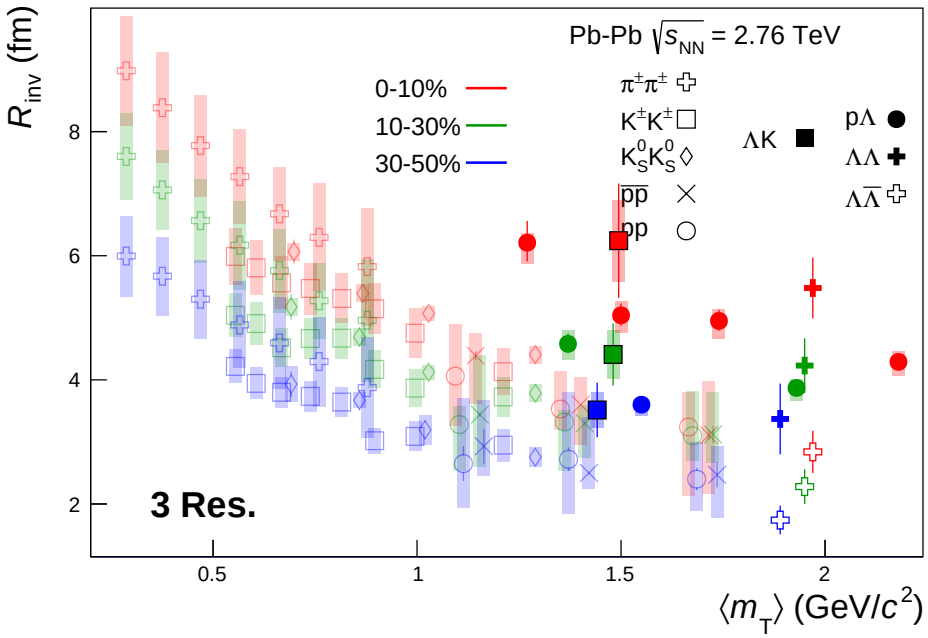

Fig. 6: 3 residual correlations in ΛK fits. Extracted fit R_{inv} parameters as a function of pair transverse mass (m_{T}) for various pair systems over several centralities. The ALICE published data [**?**] are shown with transparent, open symbols. The new ΛK results are shown with opaque, filled symbols. The m_{T} value for the ΛK system is an average of those for the $\Lambda\mathrm{K}^+$, $\bar{\Lambda}\mathrm{K}^-$, and $\Lambda\mathrm{K}^0_{\mathrm{S}}$ systems.

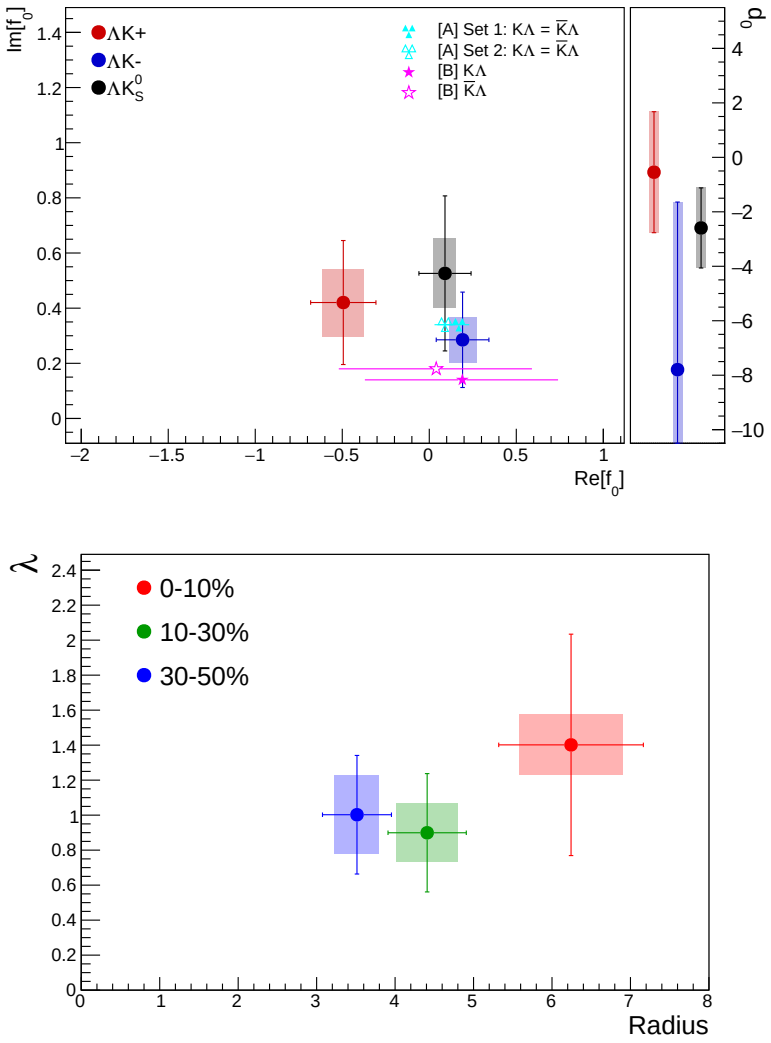

Fig. 7: Extracted fit parameters for the case of 3 residual contributors for all of our ΛK systems. [Top]: $\Im f_0$ vs. $\Re f_0$, together with d_0 to the right. [Bottom]: λ vs. Radius for the 0-10% (blue), 10-30% (green), and 30-50% (red) centrality bins. In the fit, all ΛK systems share common radii. The color scheme used in the panel are to be consistent with those in Fig. 6. The cyan ([A] = Ref. [**?**]) and magenta ([B] = Ref. [**?**]) points show theoretical predictions made using chiral perturbation theory.

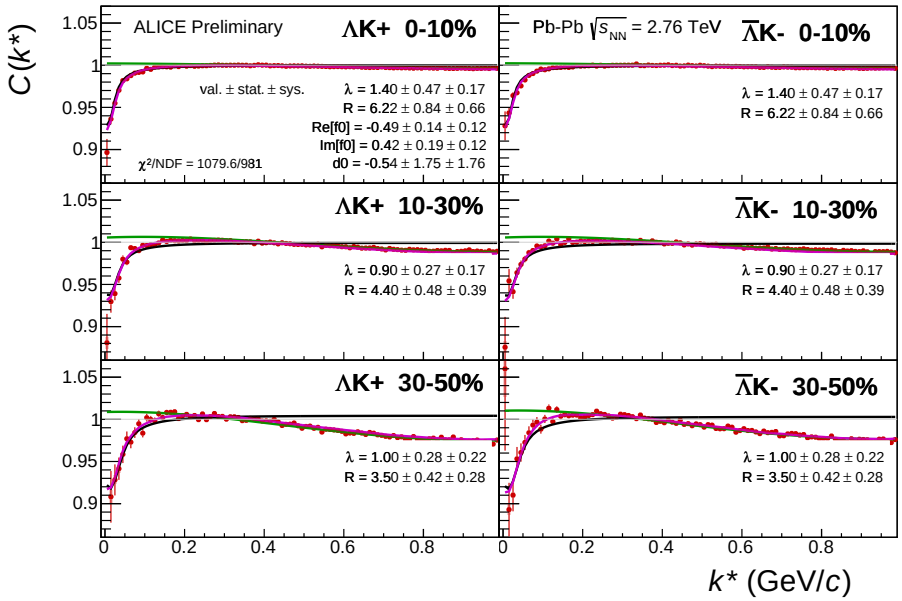

Fig. 8: Fit results, with 3 residual correlations included, for the ΛK^+ and $\bar{\Lambda} K^-$ data. The ΛK^+ data is shown in the left column, the $\bar{\Lambda} K^-$ in the right, and the rows differentiate the different centrality bins (0-10% in the top, 10-30% in the middle, and 30-50% in the bottom).

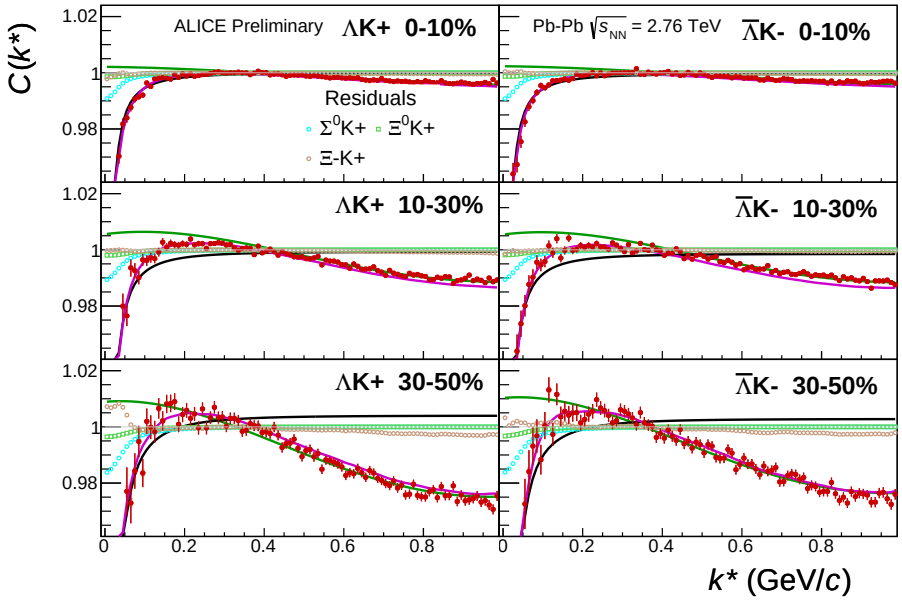

Fig. 9: Fit results with the 3 residual contributions shown, for the ΛK^+ and $\bar{\Lambda} K^-$ data. The ΛK^+ data is shown in the left column, the $\bar{\Lambda} K^-$ in the right, and the rows differentiate the different centrality bins (0-10% in the top, 10-30% in the middle, and 30-50% in the bottom).

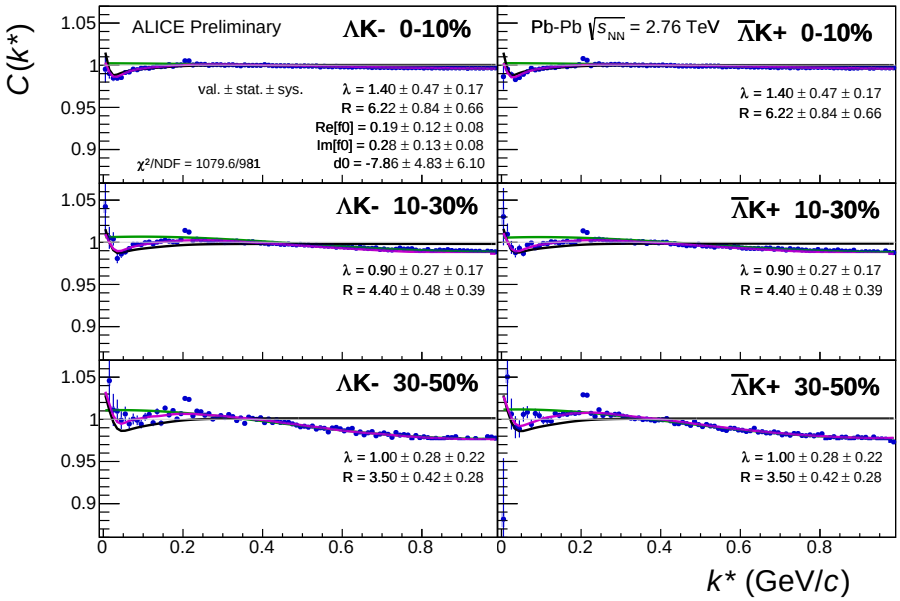

Fig. 10: Fit results, with 3 residual correlations included, for the ΛK^- and $\bar{\Lambda}K^+$ data. The ΛK^- data is shown in the left column, the $\bar{\Lambda}K^+$ in the right, and the rows differentiate the different centrality bins (0-10% in the top, 10-30% in the middle, and 30-50% in the bottom).

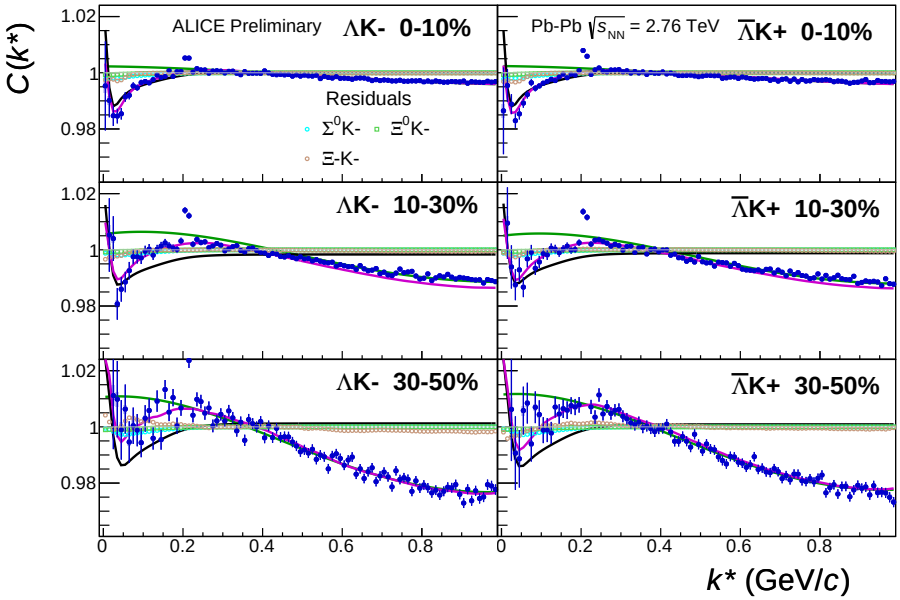

Fig. 11: Fit results with the 3 residual contributions shown, for the ΛK^- and $\bar{\Lambda}K^+$ data. The ΛK^- data is shown in the left column, the $\bar{\Lambda}K^+$ in the right, and the rows differentiate the different centrality bins (0-10% in the top, 10-30% in the middle, and 30-50% in the bottom).

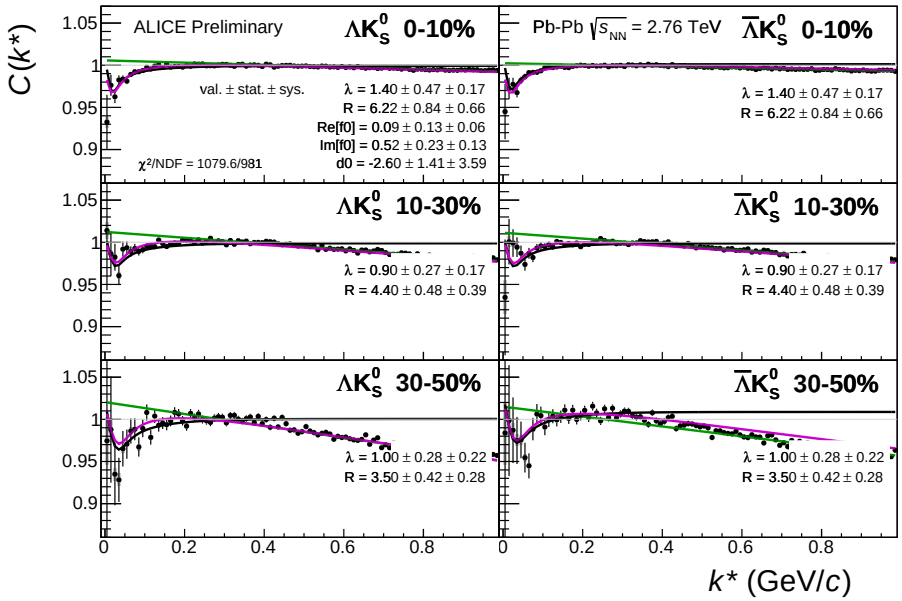

Fig. 12: Fit results, with 3 residual correlations included, for the ΛK^0_S and $\bar{\Lambda} K^0_S$ data. The ΛK^0_S data is shown in the left column, the $\bar{\Lambda} K^0_S$ in the right, and the rows differentiate the different centrality bins (0-10% in the top, 10-30% in the middle, and 30-50% in the bottom).

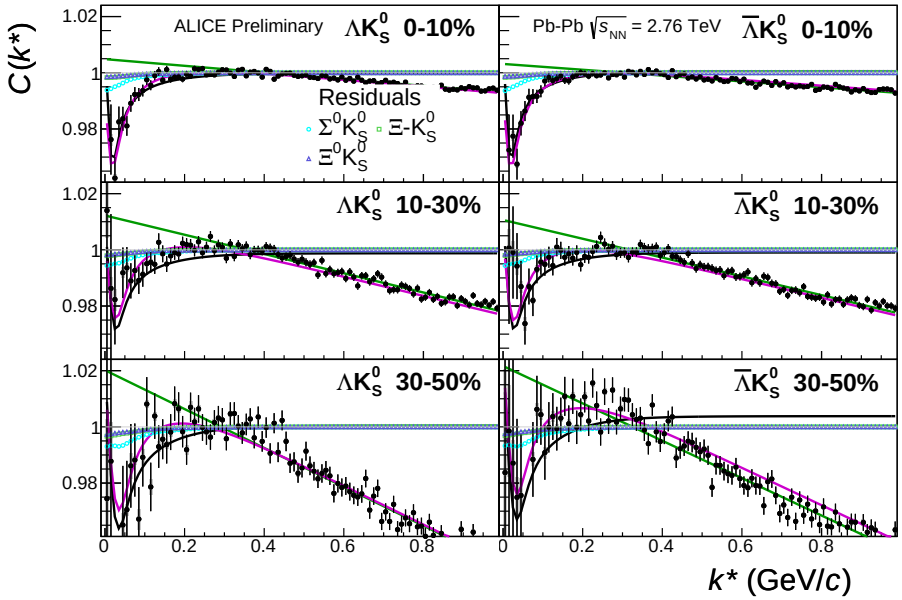

Fig. 13: Fit results with the 3 residual contributions shown, for the ΛK^0_S and $\bar{\Lambda} K^0_S$ data. The ΛK^0_S data is shown in the left column, the $\bar{\Lambda} K^0_S$ in the right, and the rows differentiate the different centrality bins (0-10% in the top, 10-30% in the middle, and 30-50% in the bottom).

1.3 10 Residual Contributors Included in Fit

This section presents fit results for which 10 residual contributors were assumed. These contributors include those shared by the three contributor case (App. 1.2), $(\Sigma^0\mathrm{K}, \Xi^0\mathrm{K}, \Xi^-\mathrm{K}) \rightarrow \Lambda\mathrm{K}$, and additionally the contributors $(\Sigma^{*(+,-,0)}\mathrm{K}^{*0}, \Lambda\mathrm{K}^{*0}, \Sigma^0\mathrm{K}^{*0}, \Xi^0\mathrm{K}^{*0}, \Xi^-\mathrm{K}^{*0}) \rightarrow \Lambda\mathrm{K}$. As stated at the beginning of App. 1, most of the Σ^* and K^* resonances will have decayed before kinetic freeze-out, and therefore it is best to treat Λ and K particles originating from these resonances as primary, i.e. only using three residual contributors. However, it is still interesting to examine how these additional shorter lived sources affect our fit result, as presented below. For a comparison of these results to the case of three residual contributors, see Fig. 1 in App. 1.1

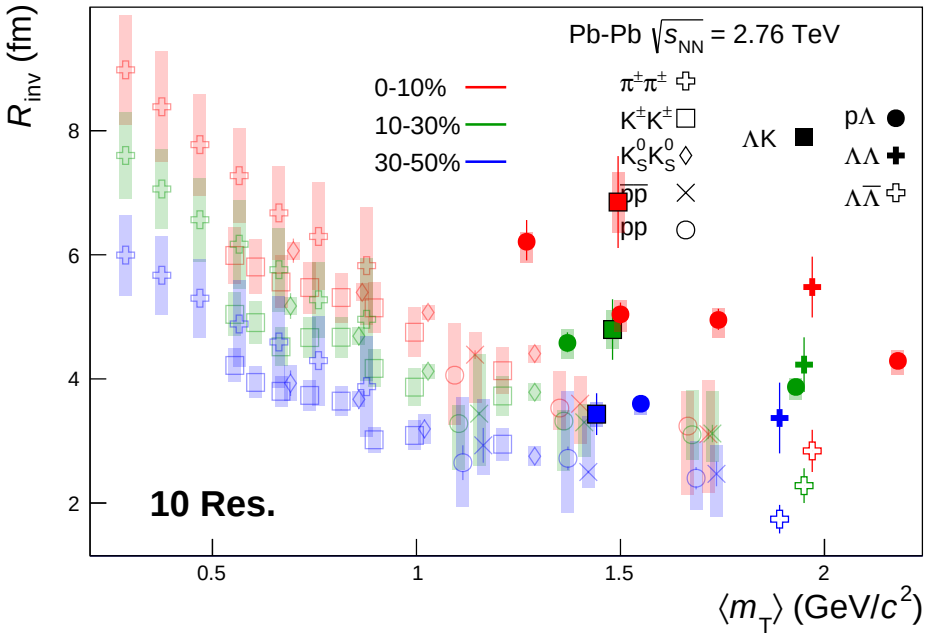

Fig. 14: 10 residual correlations in ΛK fits. Extracted fit R_{inv} parameters as a function of pair transverse mass (m_{T}) for various pair systems over several centralities. The ALICE published data [**?**] are shown with transparent, open symbols. The new ΛK results are shown with opaque, filled symbols. The m_{T} value for the ΛK system is an average of those for the $\Lambda\mathrm{K}^+$, $\bar{\Lambda}\mathrm{K}^-$, and $\Lambda\mathrm{K}^0_{\mathrm{S}}$ systems.

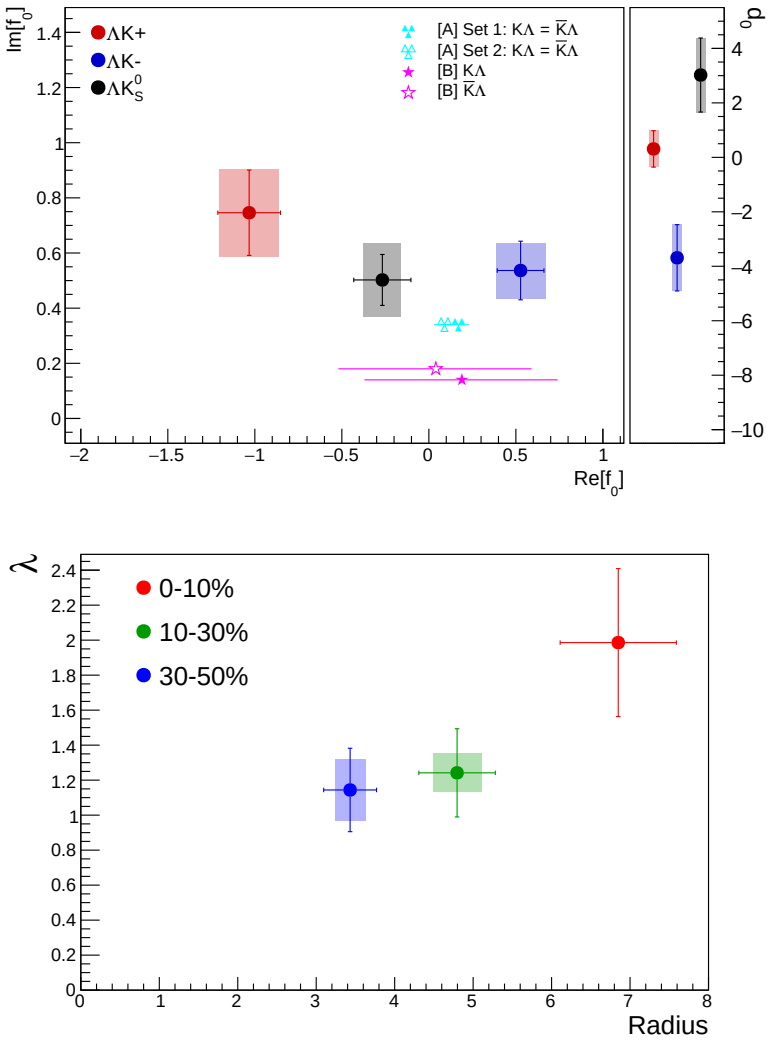

Fig. 15: Extracted fit parameters for the case of 10 residual contributors for all of our ΛK systems. [Top]: $\Im f_0$ vs. $\Re f_0$, together with d_0 to the right. [Bottom]: λ vs. Radius for the 0-10% (blue), 10-30% (green), and 30-50% (red) centrality bins. In the fit, all ΛK systems share common radii. The color scheme used in the panel are to be consistent with those in Fig. 14. The cyan ([A] = Ref. [**?**]) and magenta ([B] = Ref. [**?**]) points show theoretical predictions made using chiral perturbation theory.

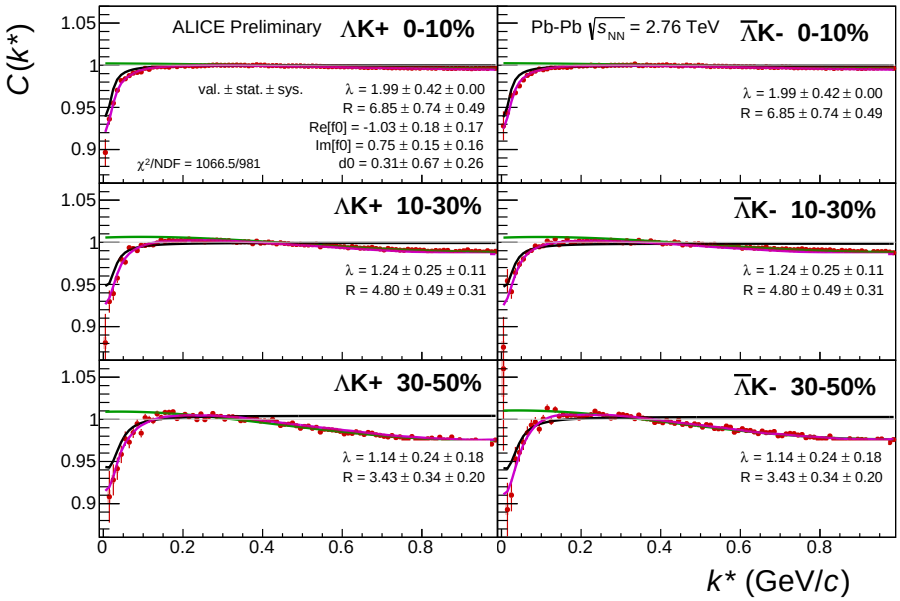

Fig. 16: Fit results, with 10 residual correlations included, for the ΛK^+ and $\bar{\Lambda}K^-$ data. The ΛK^+ data is shown in the left column, the $\bar{\Lambda}K^-$ in the right, and the rows differentiate the different centrality bins (0-10% in the top, 10-30% in the middle, and 30-50% in the bottom).

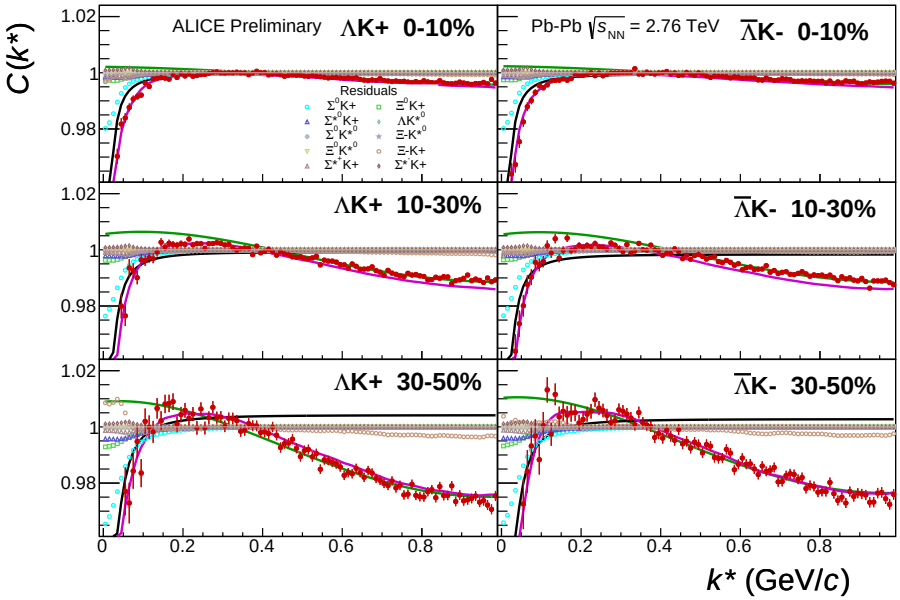

Fig. 17: Fit results with the 10 residual contributions shown, for the ΛK^+ and $\bar{\Lambda}K^-$ data. The ΛK^+ data is shown in the left column, the $\bar{\Lambda}K^-$ in the right, and the rows differentiate the different centrality bins (0-10% in the top, 10-30% in the middle, and 30-50% in the bottom).

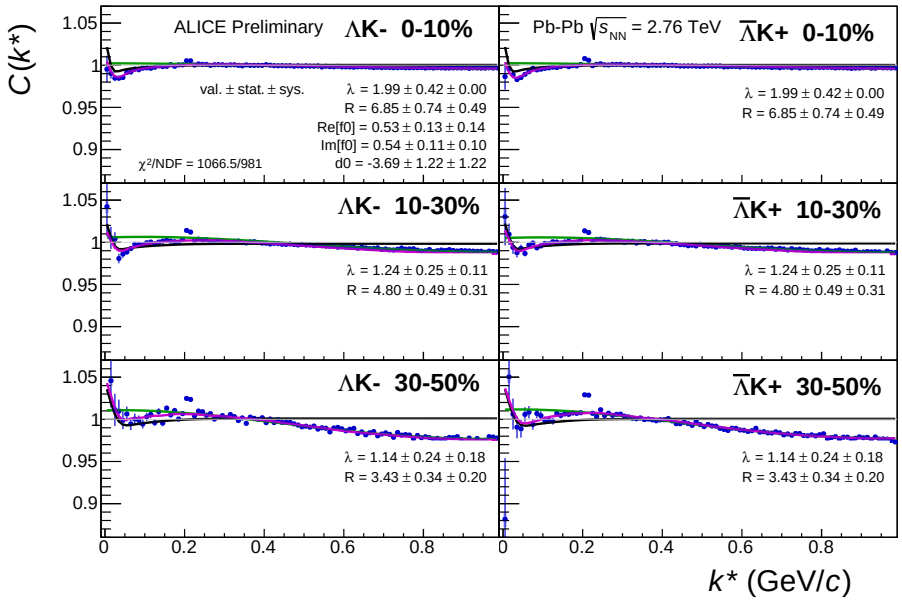

Fig. 18: Fit results, with 10 residual correlations included, for the ΛK^- and $\bar{\Lambda}K^+$ data. The ΛK^- data is shown in the left column, the $\bar{\Lambda}K^+$ in the right, and the rows differentiate the different centrality bins (0-10% in the top, 10-30% in the middle, and 30-50% in the bottom).

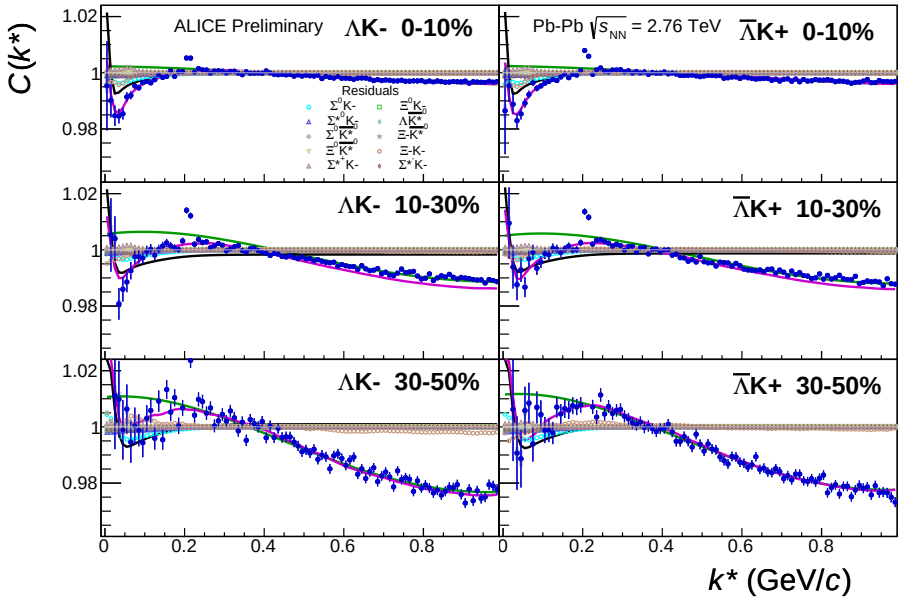

Fig. 19: Fit results with the 10 residual contributions shown, for the ΛK^- and $\bar{\Lambda}K^+$ data. The ΛK^- data is shown in the left column, the $\bar{\Lambda}K^+$ in the right, and the rows differentiate the different centrality bins (0-10% in the top, 10-30% in the middle, and 30-50% in the bottom).

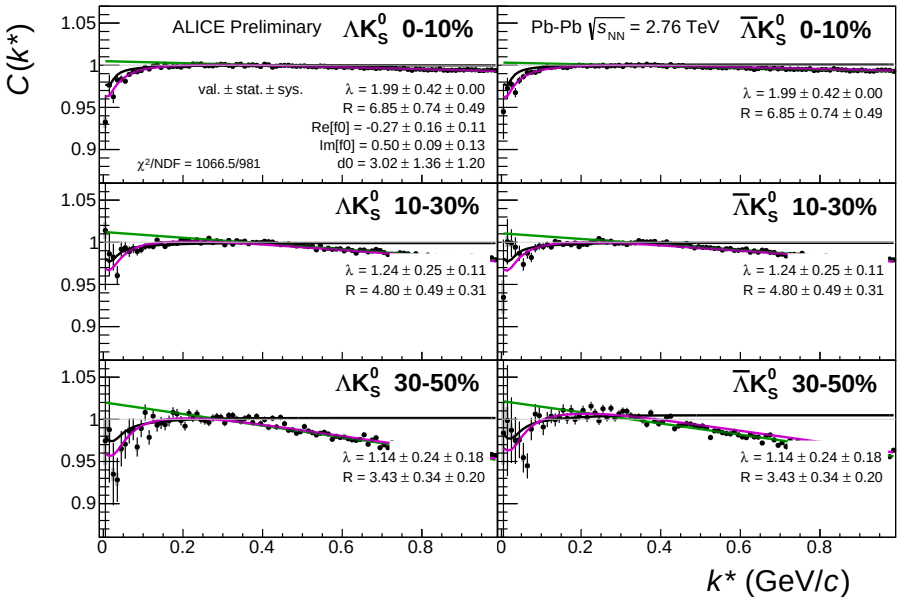

Fig. 20: Fit results, with 10 residual correlations included, for the ΛK^0_S and $\bar{\Lambda}K^0_S$ data. The ΛK^0_S data is shown in the left column, the $\bar{\Lambda}K^0_S$ in the right, and the rows differentiate the different centrality bins (0-10% in the top, 10-30% in the middle, and 30-50% in the bottom).

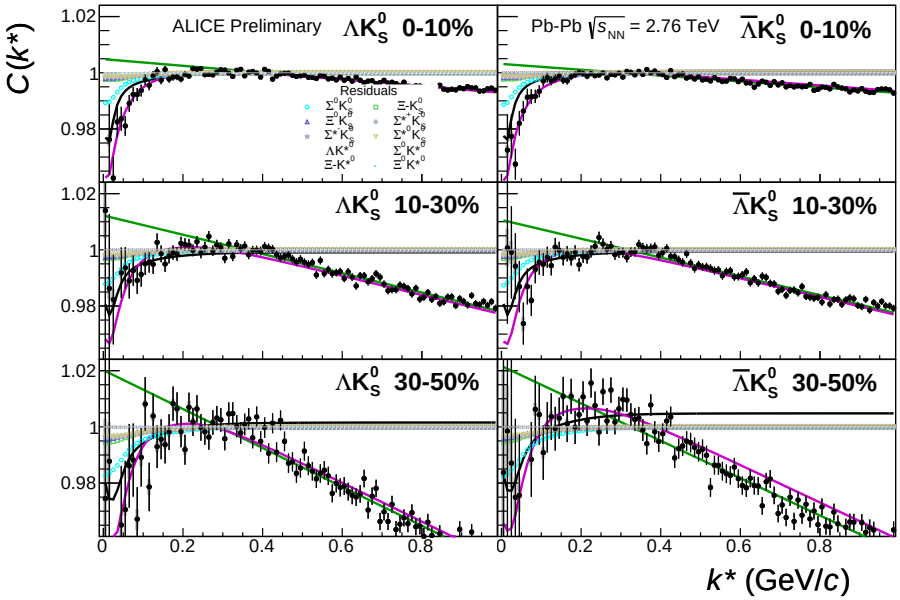

Fig. 21: Fit results with the 10 residual contributions shown, for the ΛK^0_S and $\bar{\Lambda}K^0_S$ data. The ΛK^0_S data is shown in the left column, the $\bar{\Lambda}K^0_S$ in the right, and the rows differentiate the different centrality bins (0-10% in the top, 10-30% in the middle, and 30-50% in the bottom).

1.4 No Residual Contributors Included in Fit

This section presents fit results for which no residual contributors were assumed. This is a typical starting point for femtoscopic analyses such as ours, and the effects of residual contributions are sometimes ignored. Therefore, it is interesting to observe the effects of neglecting residual feed-down from our fit description. For a comparison of these results to the case of three residual contributors, see Fig. 1 in App. 1.1

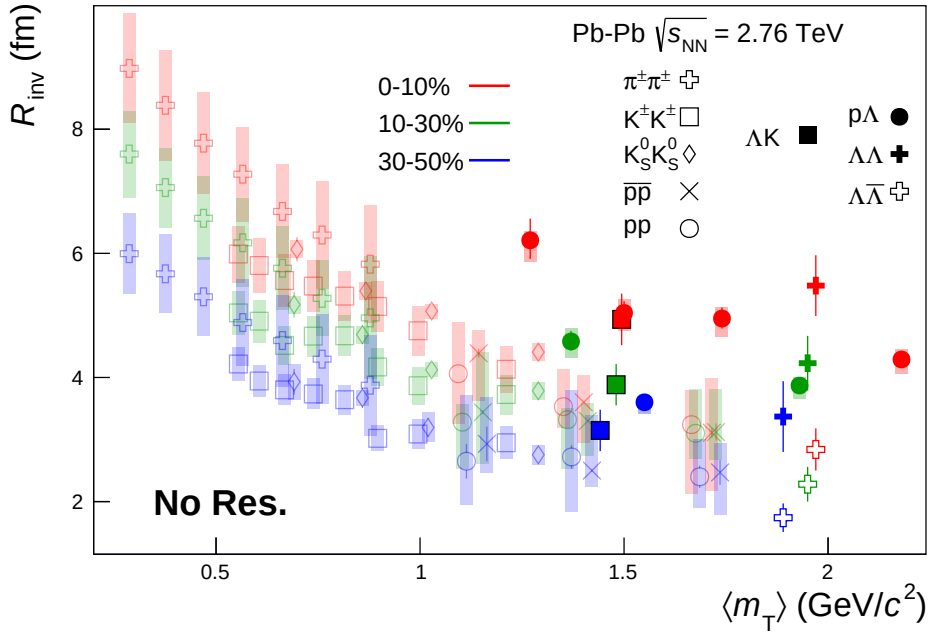

Fig. 22: No residual correlations in ΛK fits. Extracted fit $R_{\rm inv}$ parameters as a function of pair transverse mass ($m_{\rm T}$) for various pair systems over several centralities. The ALICE published data [**?**] are shown with transparent, open symbols. The new ΛK results are shown with opaque, filled symbols. The $m_{\rm T}$ value for the ΛK system is an average of those for the ΛK^+, $\bar{\Lambda} K^-$, and ΛK^0_S systems.

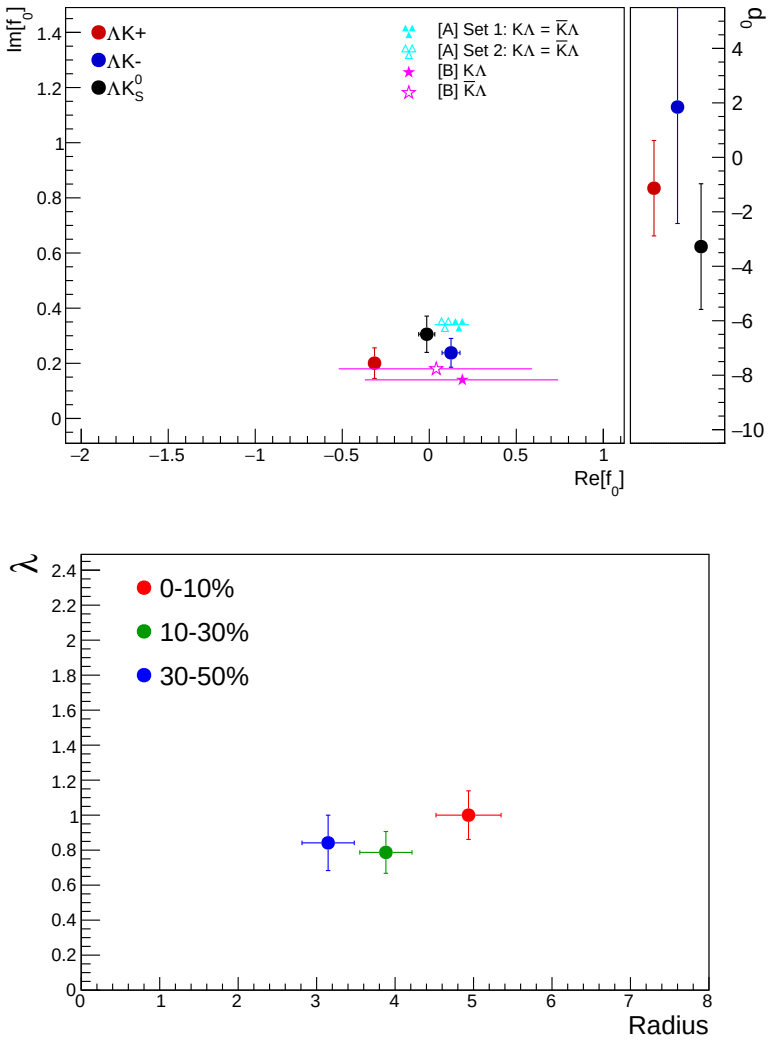

Fig. 23: Extracted fit parameters for the case of no residual contributors for all of our ΛK systems. [Top]: $\Im f_0$ vs. $\Re f_0$, together with d_0 to the right. [Bottom]: λ vs. Radius for the 0-10% (blue), 10-30% (green), and 30-50% (red) centrality bins. In the fit, all ΛK systems share common radii. The color scheme used in the panel are to be consistent with those in Fig. 22. The cyan ([A] = Ref. [**?**]) and magenta ([B] = Ref. [**?**]) points show theoretical predictions made using chiral perturbation theory.

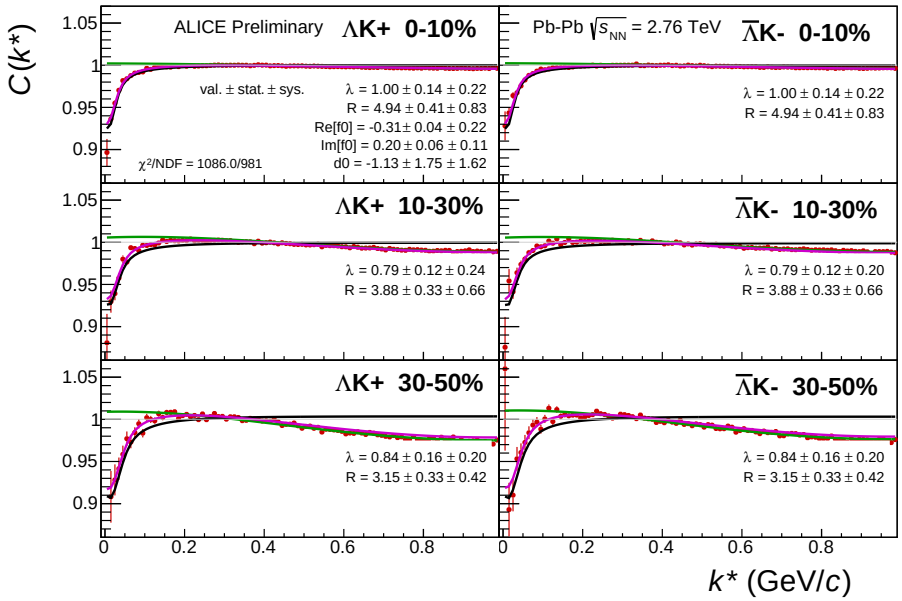

Fig. 24: Fit results, with no residual correlations included, for the ΛK^+ and $\bar{\Lambda} K^-$ data. The ΛK^+ data is shown in the left column, the $\bar{\Lambda} K^-$ in the right, and the rows differentiate the different centrality bins (0-10% in the top, 10-30% in the middle, and 30-50% in the bottom).

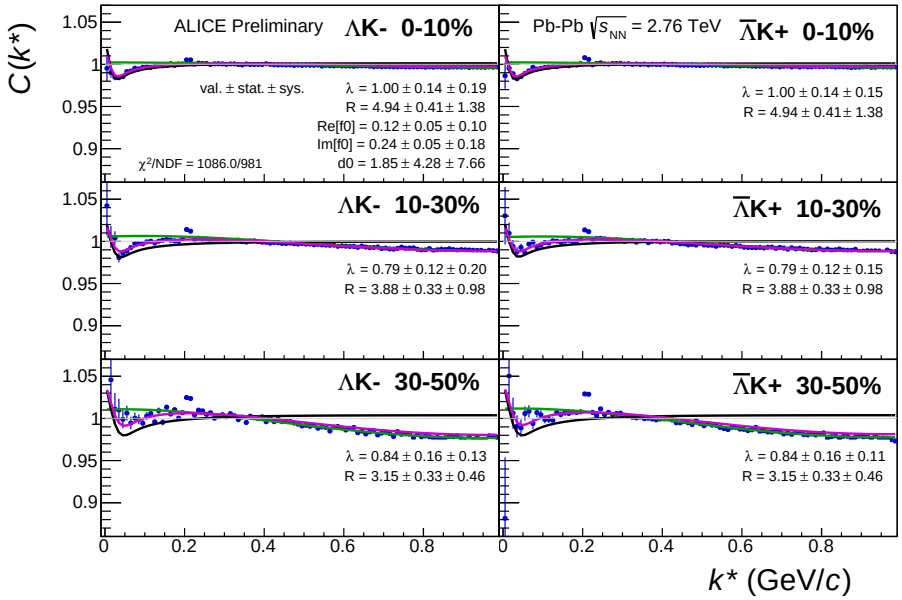

Fig. 25: Fit results, with no residual correlations included, for the ΛK^- and $\bar{\Lambda} K^+$ data. The ΛK^- data is shown in the left column, the $\bar{\Lambda} K^+$ in the right, and the rows differentiate the different centrality bins (0-10% in the top, 10-30% in the middle, and 30-50% in the bottom).

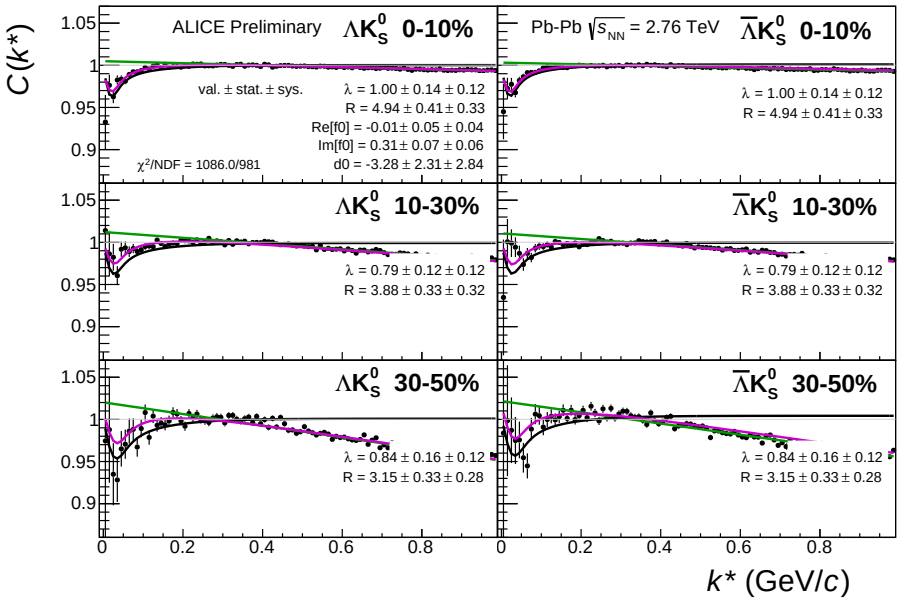

Fig. 26: Fit results, with no residual correlations included, for the ΛK^0_S and $\bar{\Lambda} K^0_S$ data. The ΛK^0_S data is shown in the left column, the $\bar{\Lambda} K^0_S$ in the right, and the rows differentiate the different centrality bins (0-10% in the top, 10-30% in the middle, and 30-50% in the bottom).

2 Spherical Harmonics

This appendix shows a spherical harmonic decomposition of our ΛK^0_S correlation functions; see Sec. **??** for a more detailed introduction to spherical harmonics in femtoscopy. For our purposes, the most interesting components are C_{00} and $\Re C_{11}$, which are presented in Figures 27 - 29. In each of the figures, the left column shows C_{00}, the right column $\Re C_{11}$, and the rows separate the centrality bins. For the the 0-10% bin, results are also included from a THERMINATOR 2 simulation for an impact parameter $b = 2$ fm (gold stars) and assumed scattering parameters ($\Re f_0$, $\Im f_0$, d_0) = (-1.16, 0.51, 1.08), (0.41, 0.47, -4.89), and (-0.41, 0.20, 2.08) for the ΛK^+, ΛK^-, and ΛK^0_S systems, respectively. The coefficient C_{00} quantifies the overall angle-integrated strength of the correlation function, similar to that studied in our 1D analysis. The $\Re C_{11}$ term is sensitive to the asymmetry in the outward direction, a component interesting for non-identical particle studies. In our analysis, we have taken the Λ to be the first particle in our pairs, and a negative value of $\Re C_{11}$ signifies the Λ particles are emitted, on average, further out and/or earlier than the K mesons. For completeness, the first six components of the spherical harmonic decompositions are shown in Figures 30 - 32

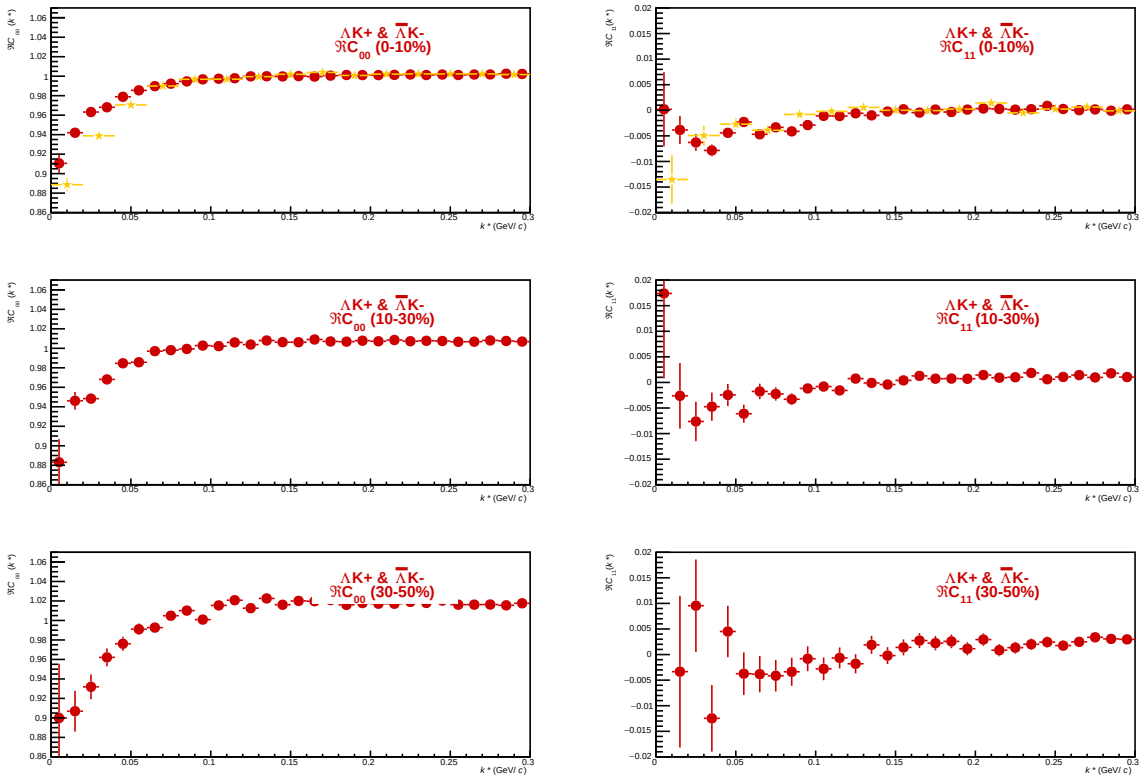

Fig. 27: C_{00} (left) and $\Re C_{11}$ (right) components of a spherical harmonic decomposition of the ΛK^+ correlation function for the 0-10% (top), 10-30% (middle), and 30-50% (bottom) centrality bins. For the the 0-10% bin, results are also included from a THERMINATOR 2 simulation for an impact parameter $b = 2$ fm (gold stars) and assumed scattering parameters ($\Re f_0$, $\Im f_0$, d_0) = (-1.16, 0.51, 1.08).

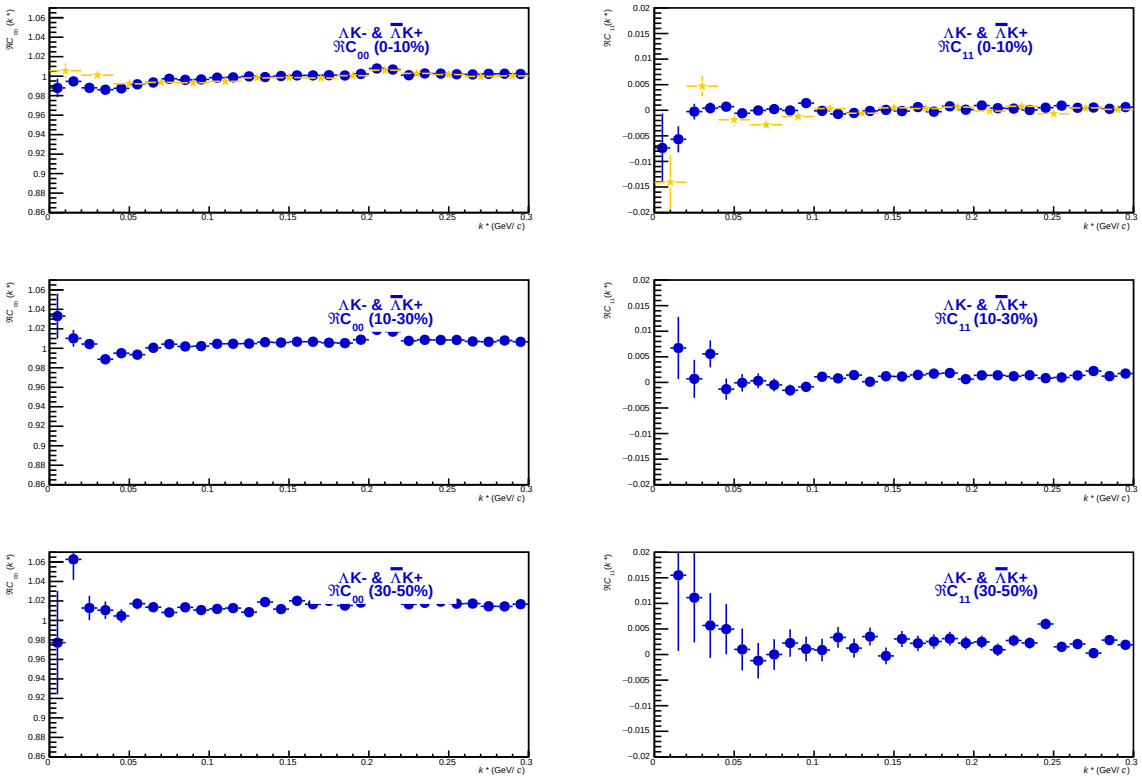

Fig. 28: C_{00} (left) and $\Re C_{11}$ (right) components of a spherical harmonic decomposition of the ΛK^- correlation function for the 0-10% (top), 10-30% (middle), and 30-50% (bottom) centrality bins. For the the 0-10% bin, results are also included from a THERMINATOR 2 simulation for an impact parameter $b = 2$ fm (gold stars) and assumed scattering parameters ($\Re f_0$, $\Im f_0$, d_0) = (0.41, 0.47, -4.89).

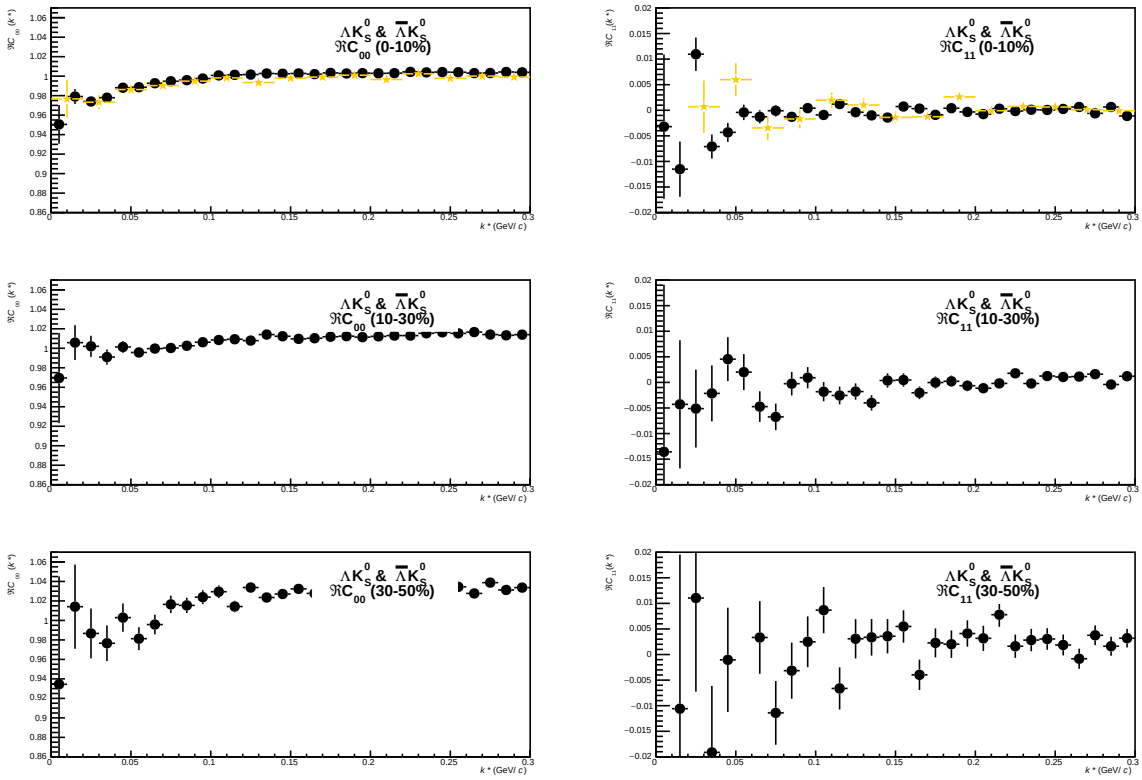

Fig. 29: C_{00} (left) and $\Re C_{11}$ (right) components of a spherical harmonic decomposition of the $\Lambda\mathrm{K}^0_\mathrm{S}$ correlation function for the 0-10% (top), 10-30% (middle), and 30-50% (bottom) centrality bins. For the the 0-10% bin, results are also included from a THERMINATOR 2 simulation for an impact parameter $b = 2$ fm (gold stars) and assumed scattering parameters ($\Re f_0$, $\Im f_0$, d_0) = (-0.41, 0.20, 2.08).

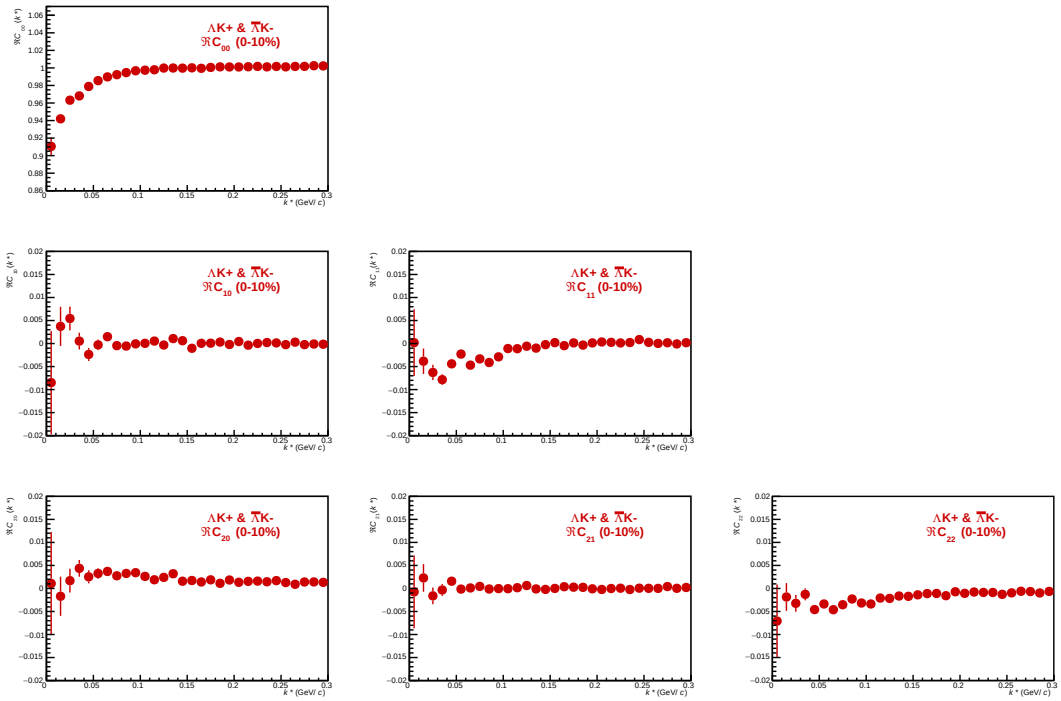

(a) Real components, $\Re C_{lm}$

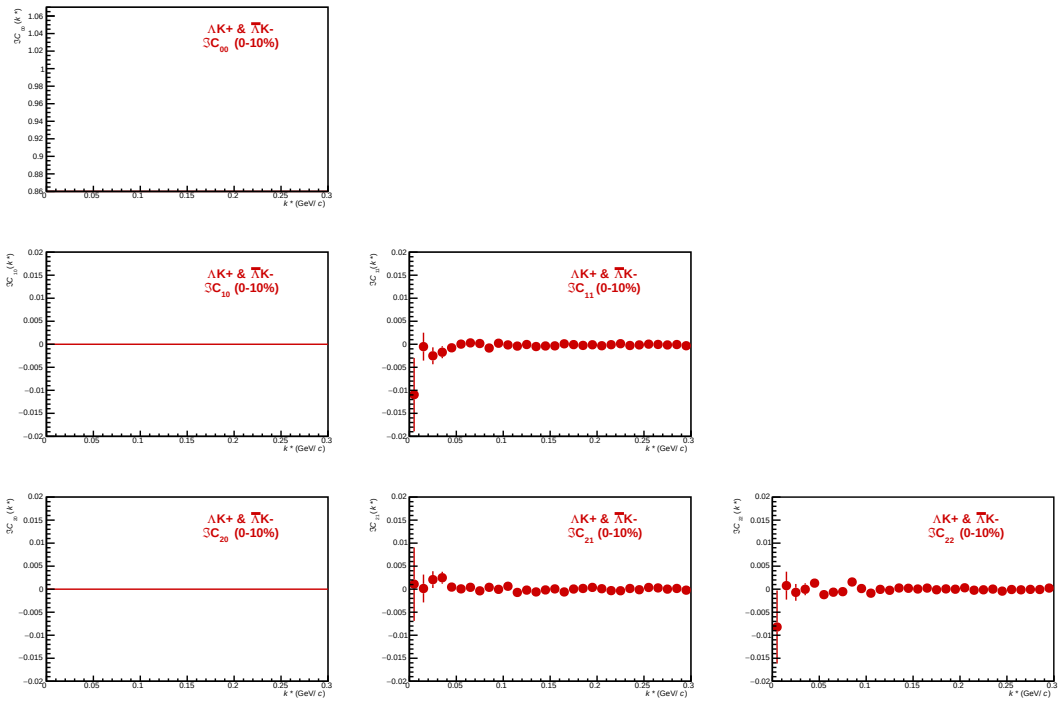

(b) Imaginary components, $\Im C_{lm}$

Fig. 30: First six components ($C_{00}, C_{10}, C_{11}, C_{20}, C_{21}, C_{22}$) of the spherical harmonic decomposition of the ΛK^+ correlation function for the 0-10% centrality bin. Note, $\Im C_{00}$, $\Im C_{10}$, and $\Im C_{20}$ are zero by definition.

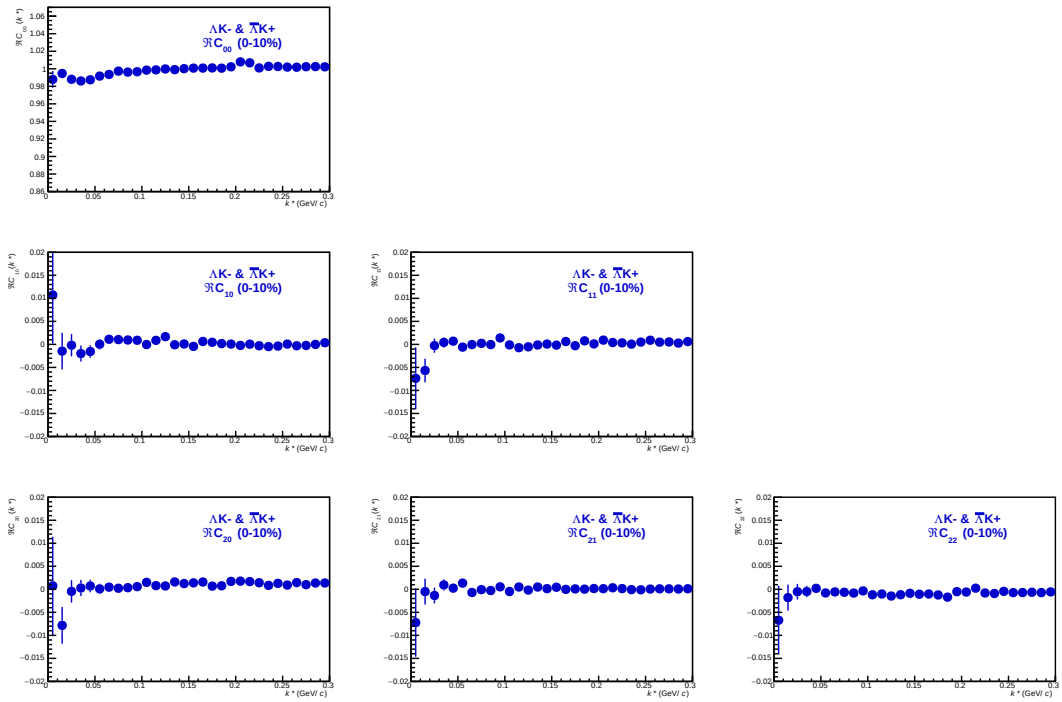

(a) Real components, $\Re C_{lm}$

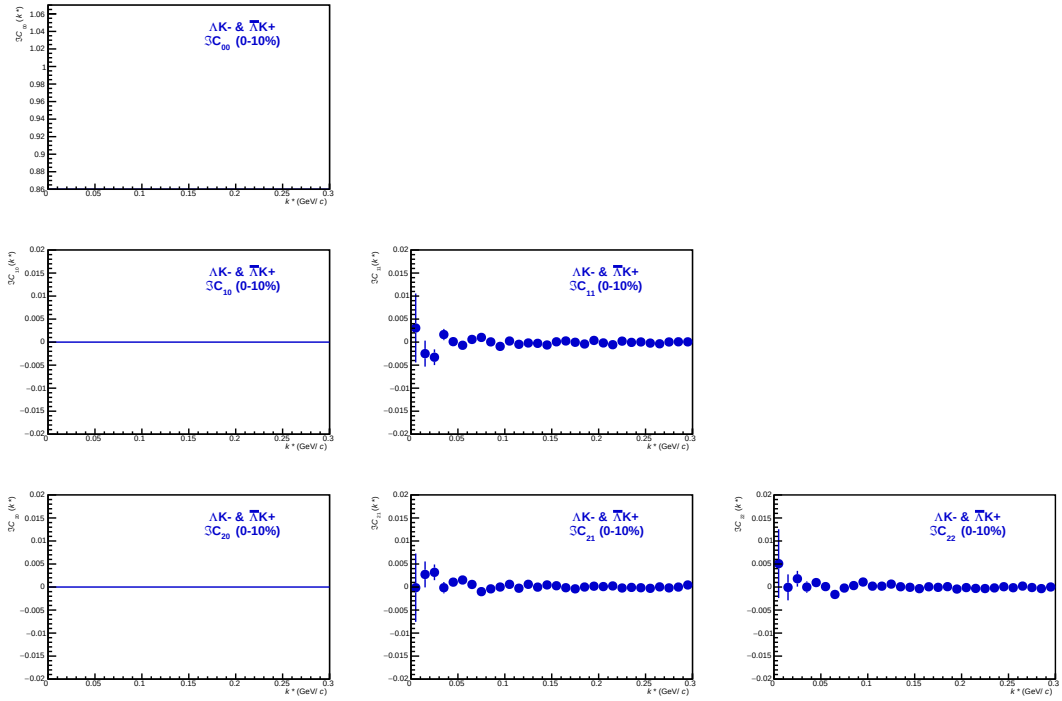

(b) Imaginary components, $\Im C_{lm}$

Fig. 31: First six components ($C_{00}, C_{10}, C_{11}, C_{20}, C_{21}, C_{22}$) of the spherical harmonic decomposition of the ΛK^- correlation function for the 0-10% centrality bin. Note, $\Im C_{00}$, $\Im C_{10}$, and $\Im C_{20}$ are zero by definition.

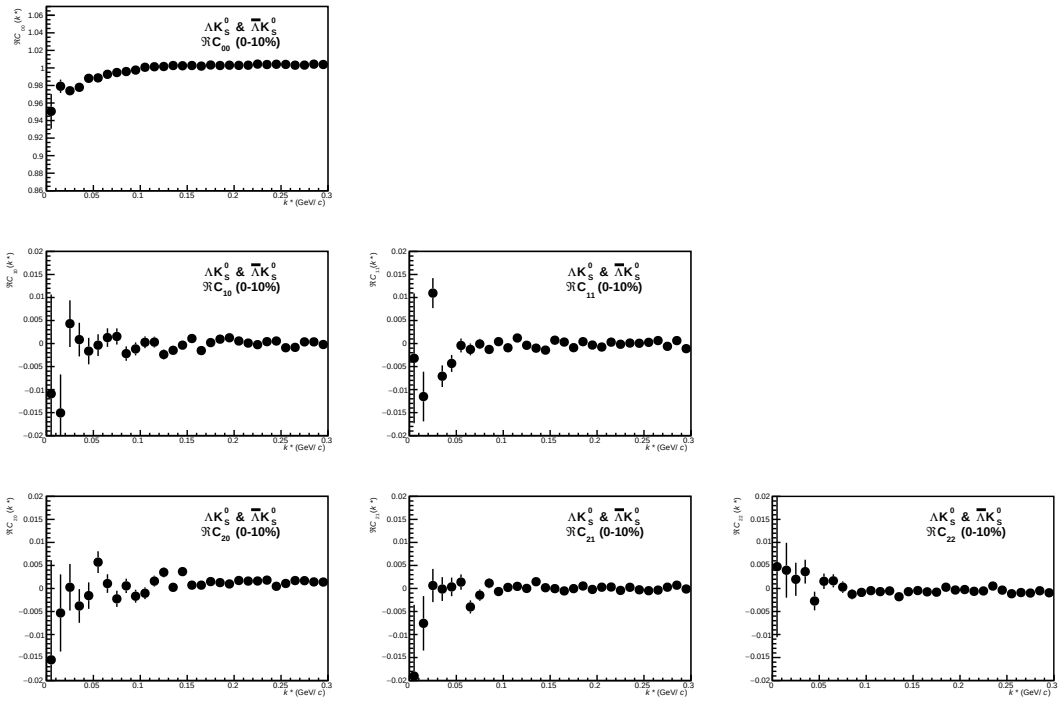

(a) Real components, $\Re C_{lm}$

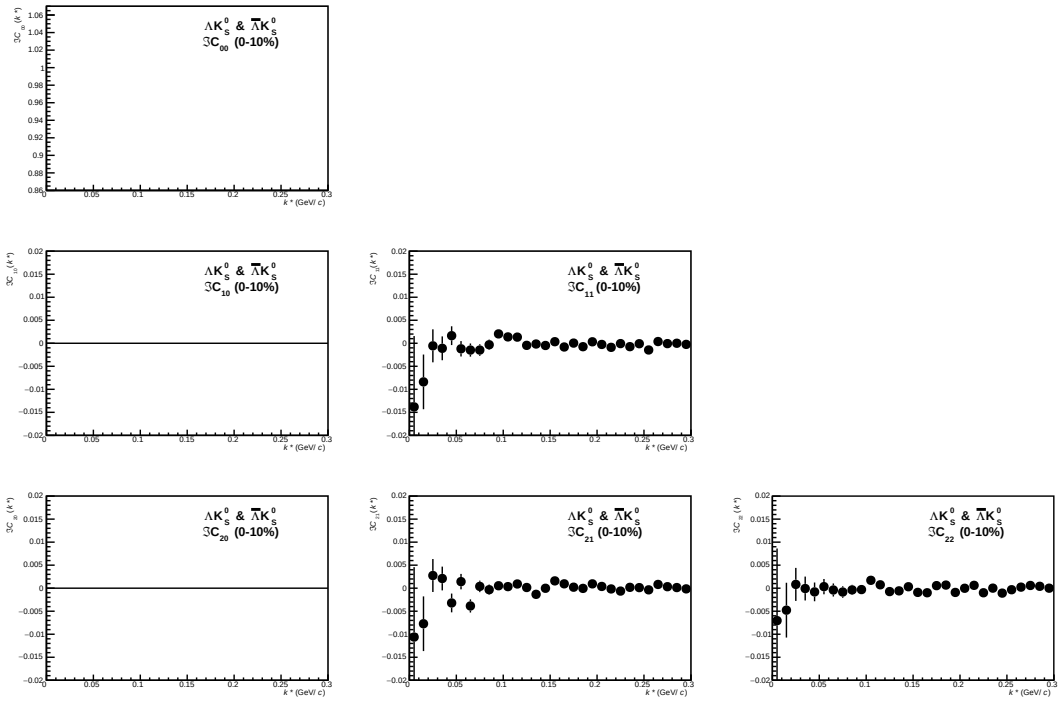

(b) Imaginary components, $\Im C_{lm}$

Fig. 32: First six components ($C_{00}, C_{10}, C_{11}, C_{20}, C_{21}, C_{22}$) of the spherical harmonic decomposition of the $\Lambda\mathrm{K}^0_\mathrm{S}$ correlation function for the 0-10% centrality bin. Note, $\Im C_{00}$, $\Im C_{10}$, and $\Im C_{20}$ are zero by definition.

3 Additional Figures

3.1 Residuals

3.1.1 ΛK^+ Residuals

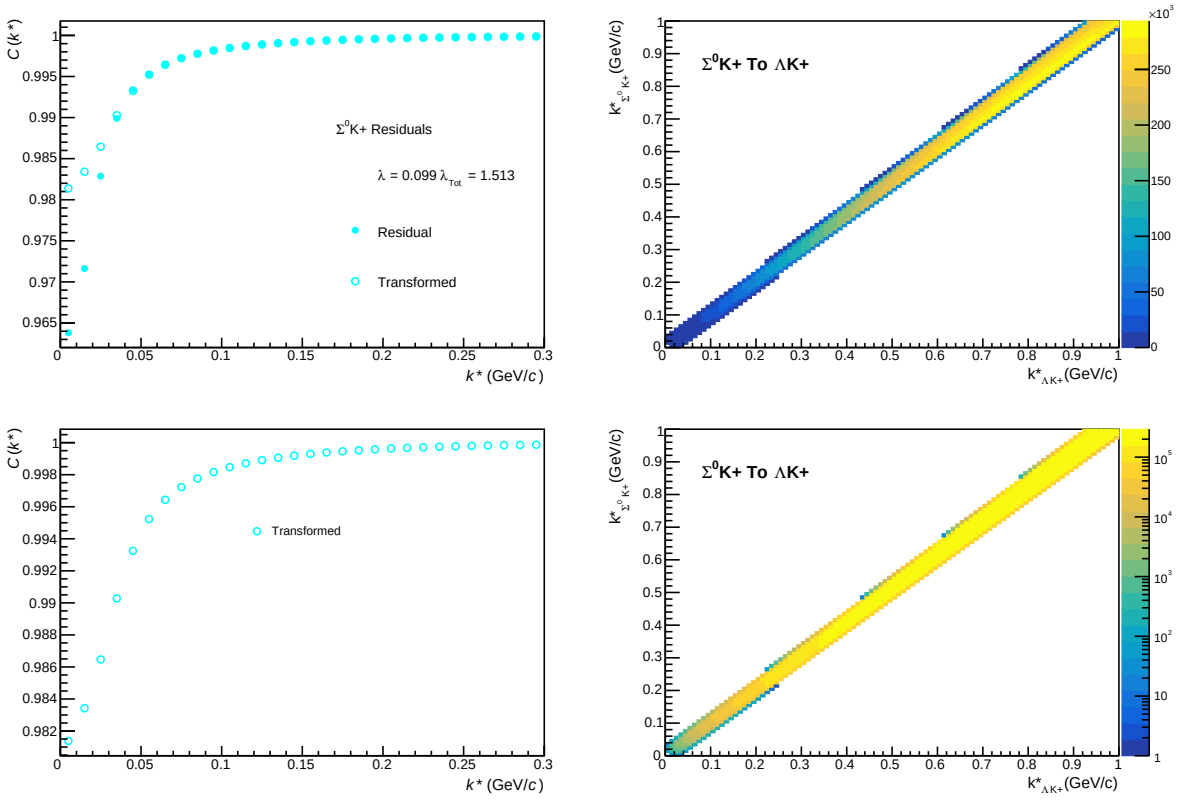

Fig. 33: Residuals: $\Sigma^0 K^+$ to ΛK^+ (0-10% Centrality)

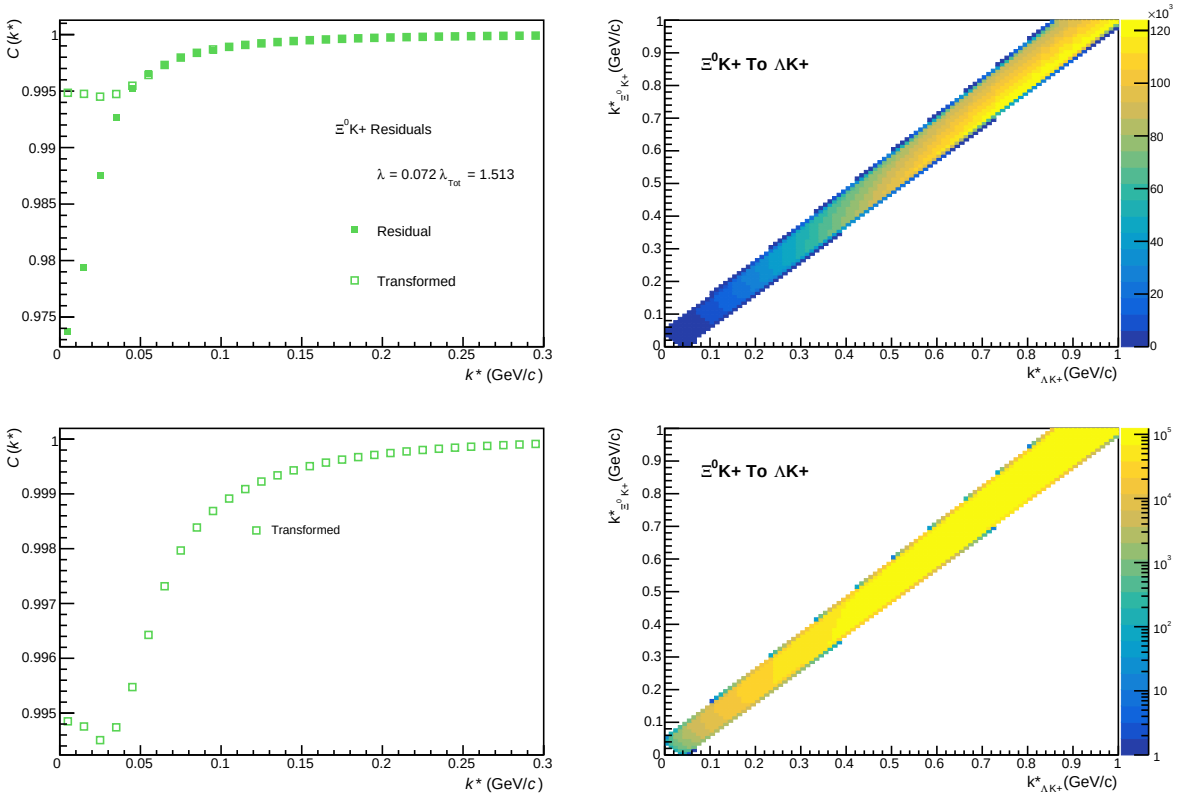

Fig. 34: Residuals: $\Xi^0 K^+$ to ΛK^+ (0-10% Centrality)

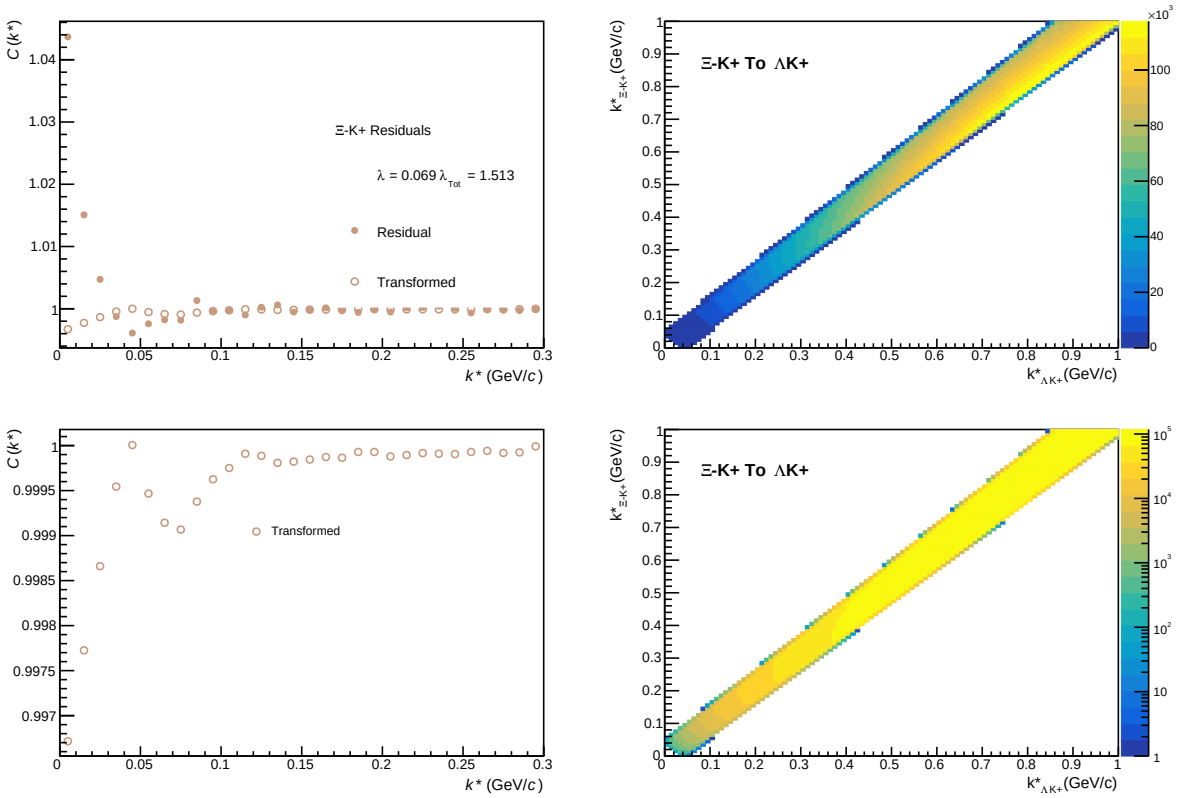

Fig. 35: Residuals: $\Xi^- K^+$ to ΛK^+ (0-10% Centrality)

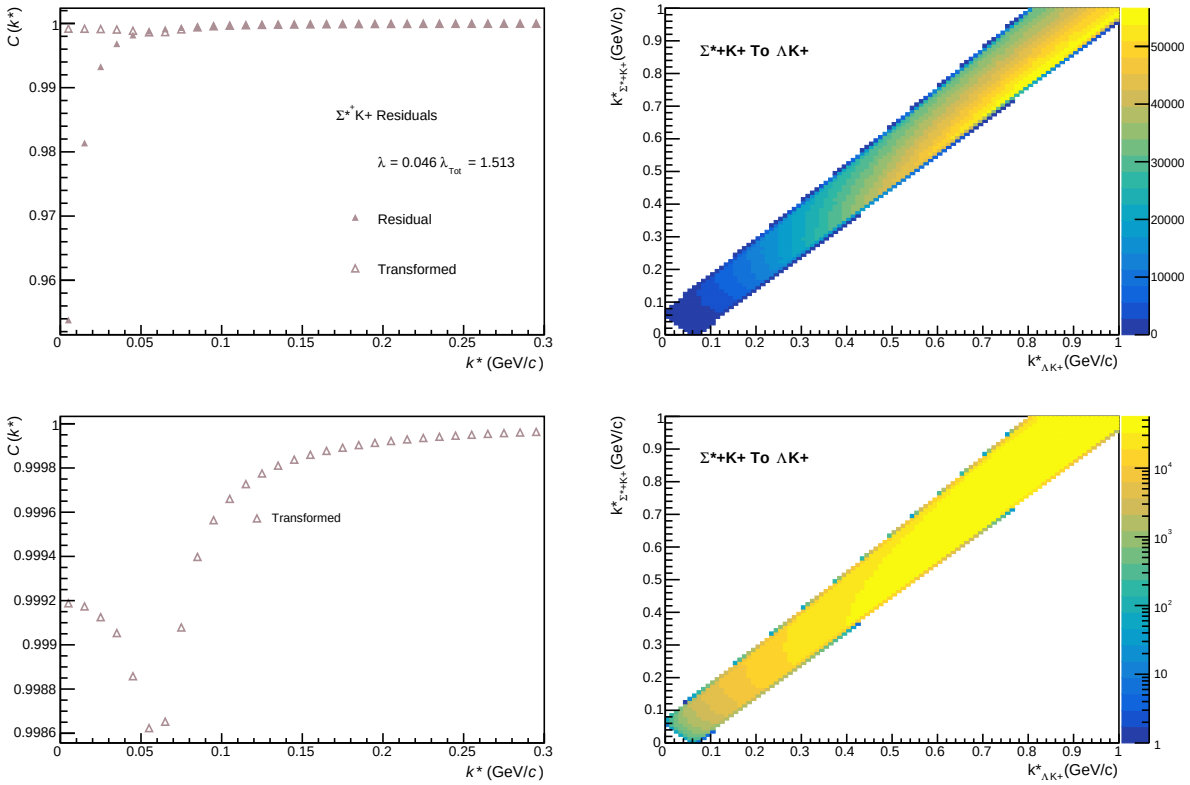

Fig. 36: Residuals: $\Sigma^{*+}K^{+}$ to ΛK^{+} (0-10% Centrality)

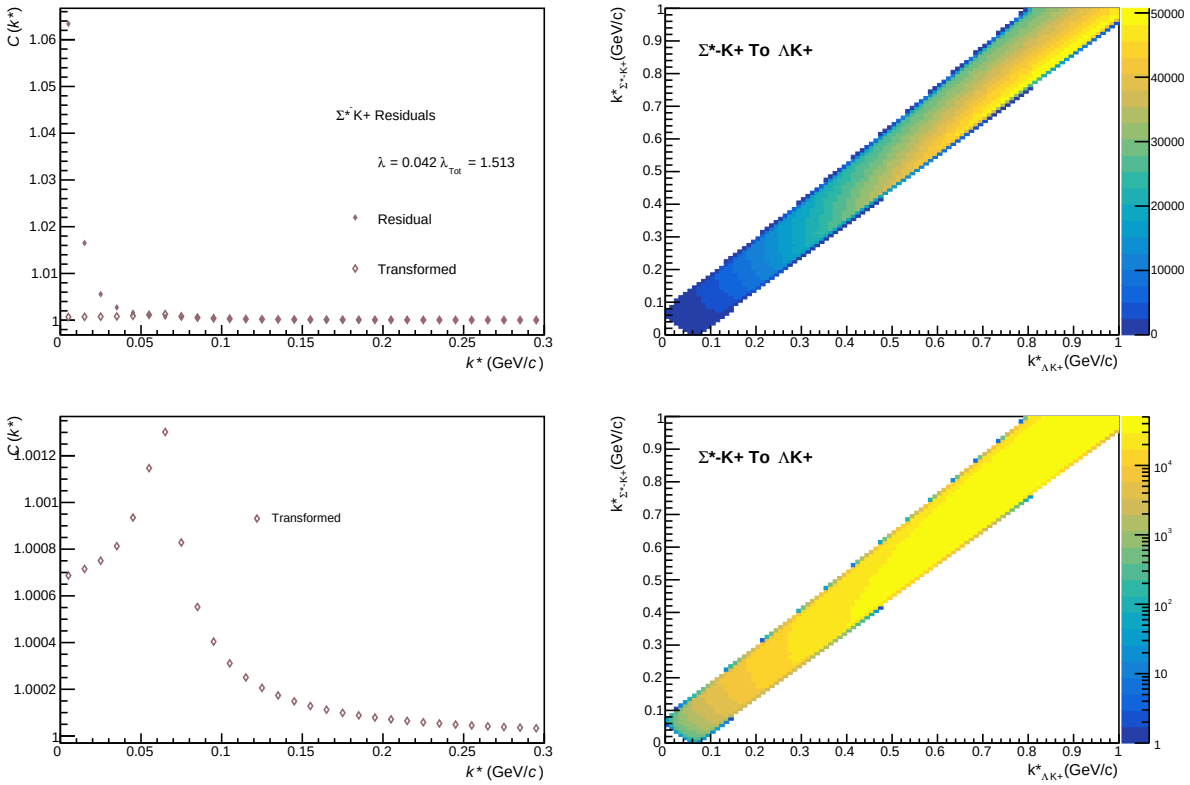

Fig. 37: Residuals: $\Sigma^{*-}K^{+}$ to ΛK^{+} (0-10% Centrality)

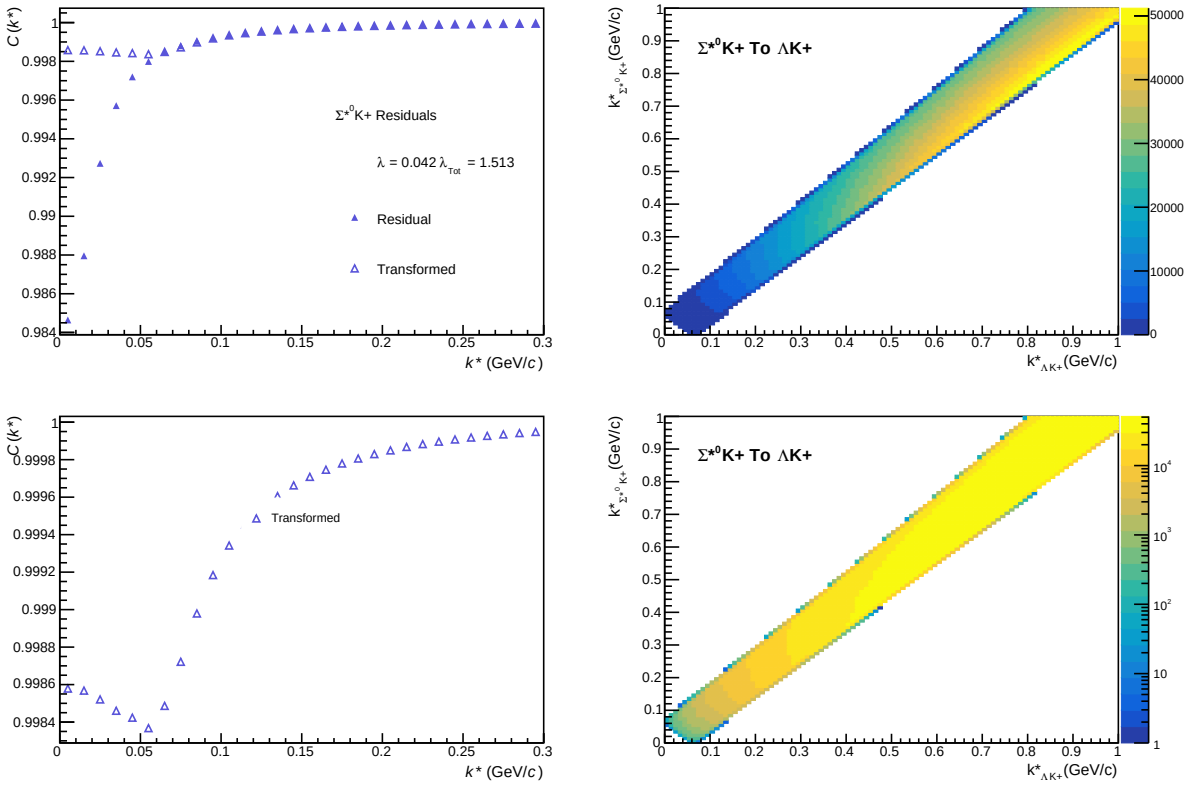

Fig. 38: Residuals: $\Sigma^{*0}K^{+}$ to ΛK^{+} (0-10% Centrality)

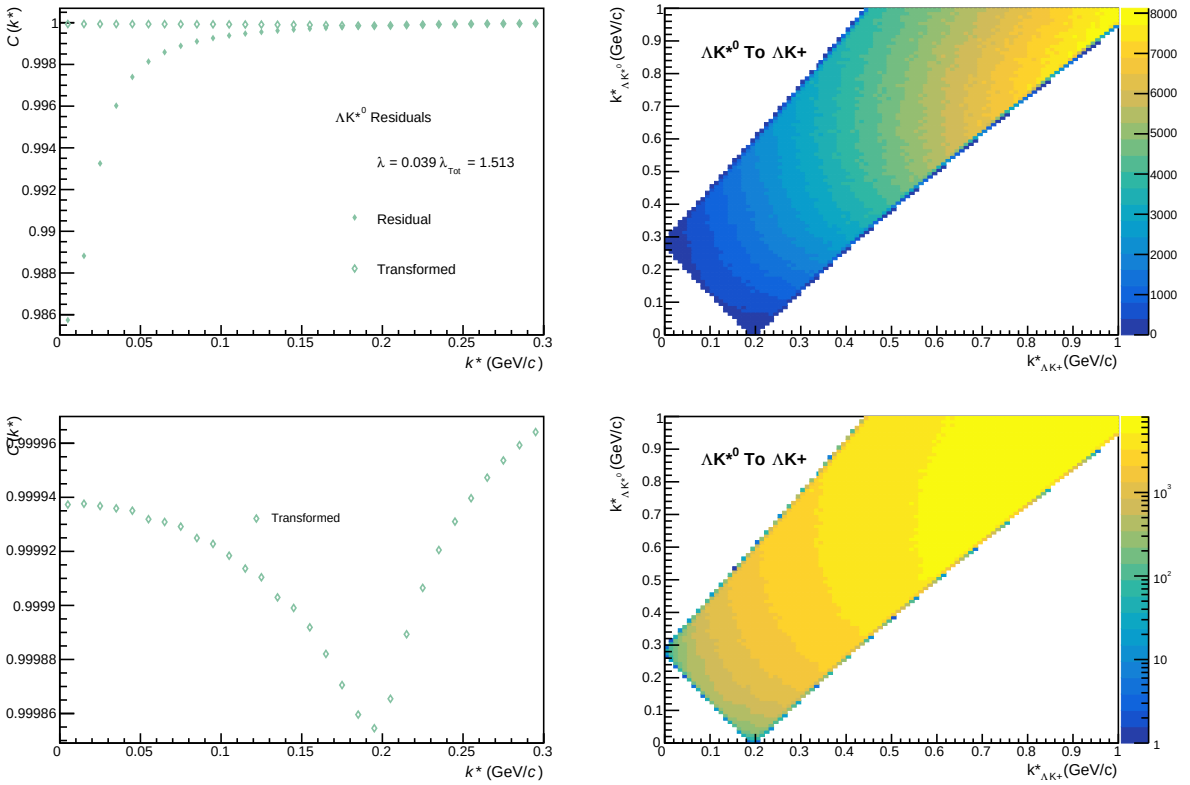

Fig. 39: Residuals: ΛK^{*0} to ΛK^{+} (0-10% Centrality)

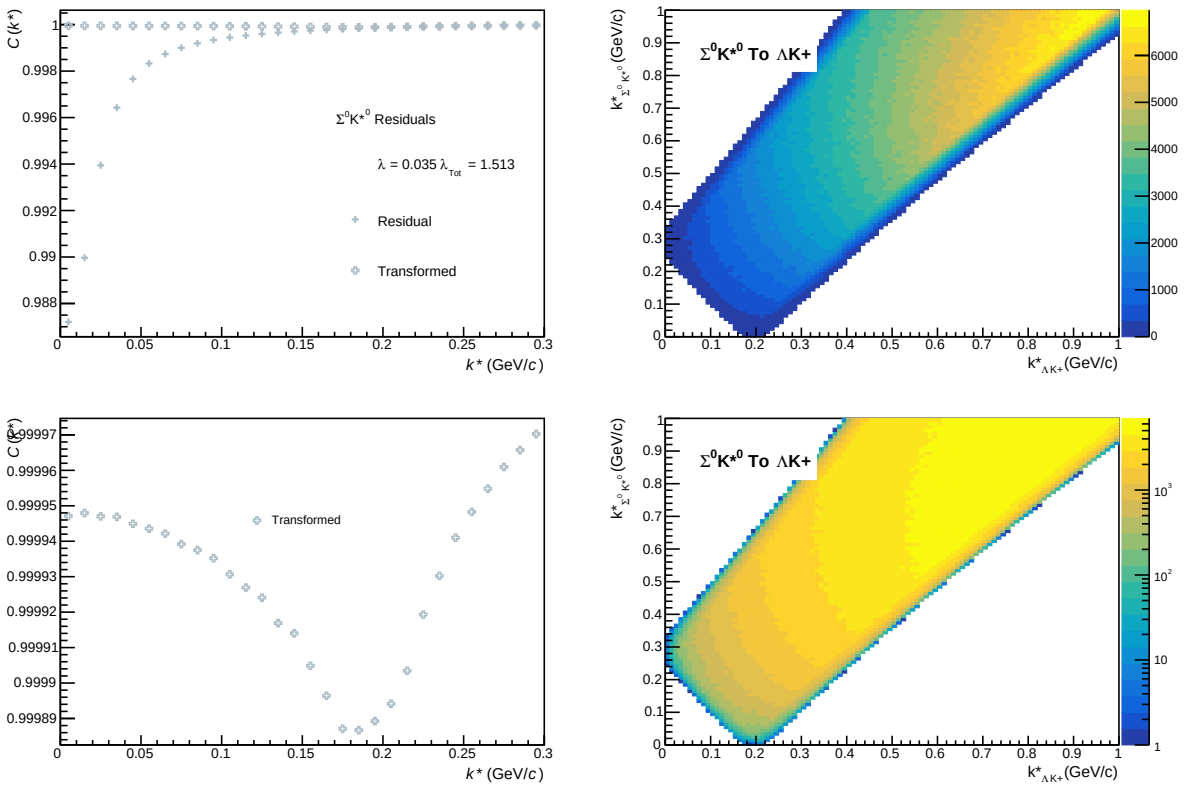

Fig. 40: Residuals: $\Sigma^0 K^{*0}$ to ΛK^+ (0-10% Centrality)

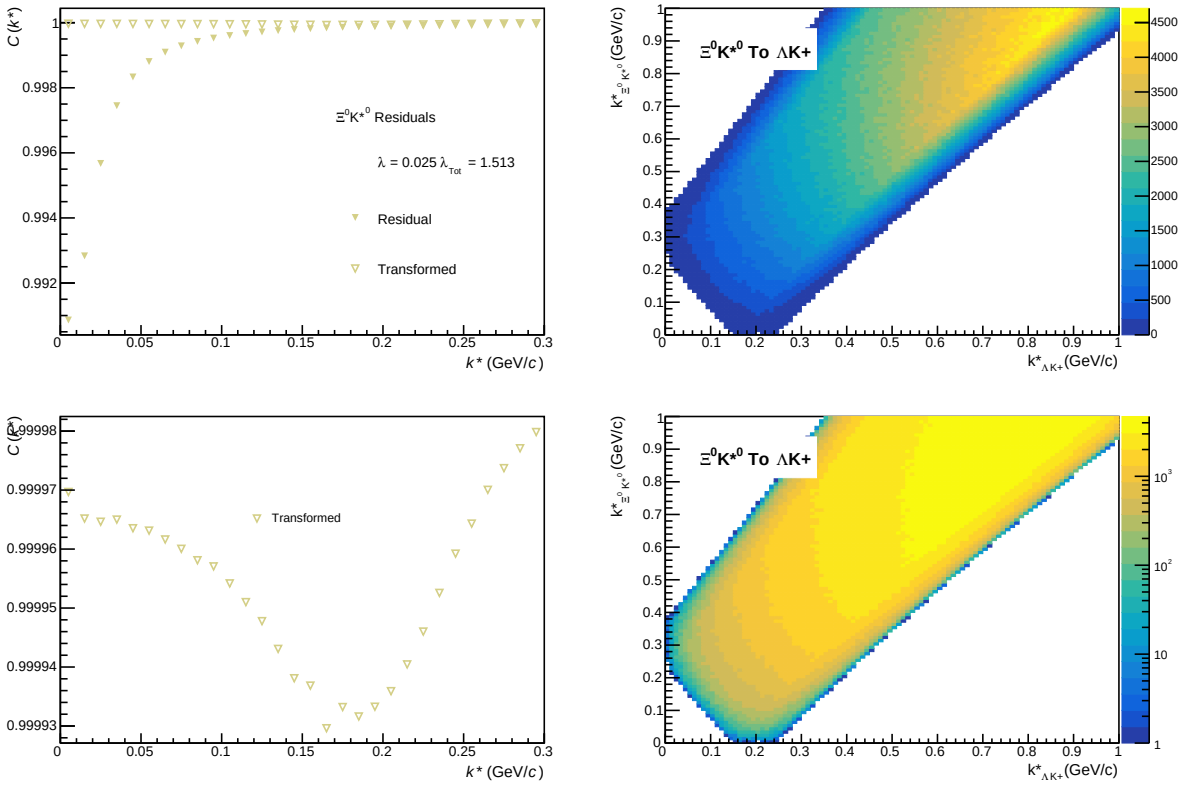

Fig. 41: Residuals: $\Xi^0 K^{*0}$ to ΛK^+ (0-10% Centrality)

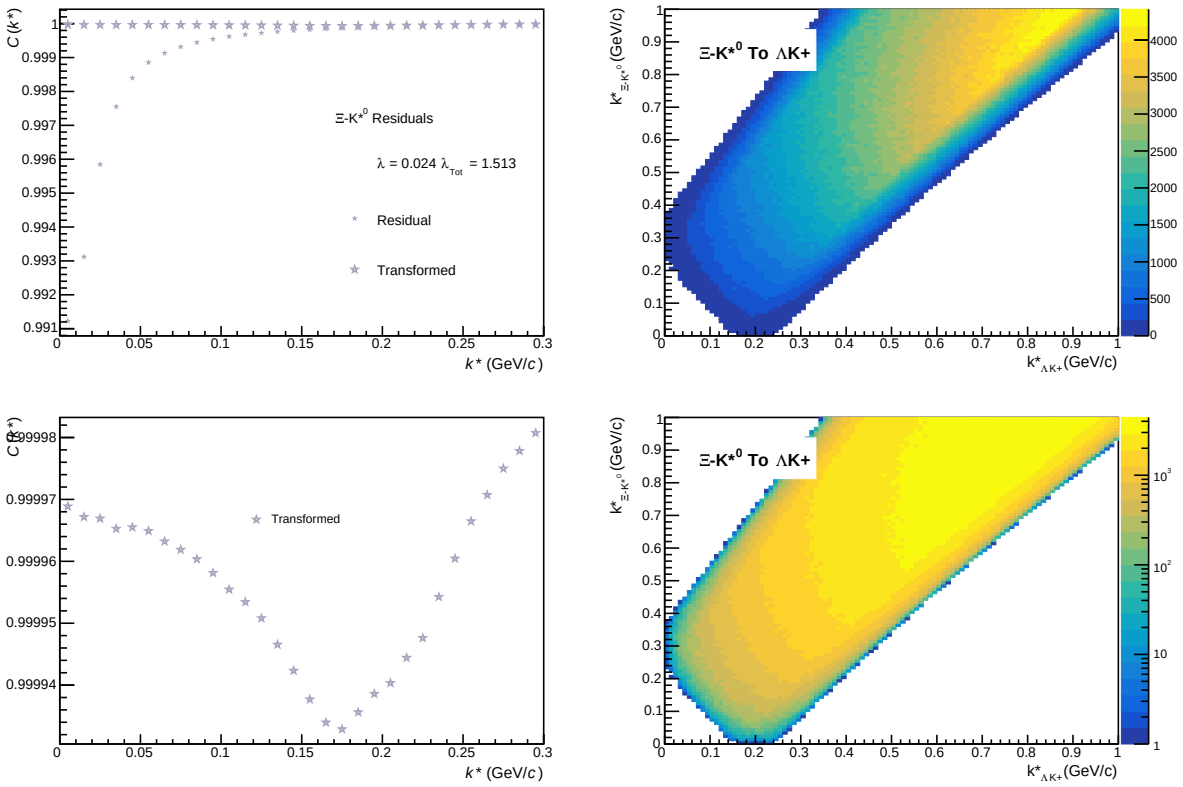

Fig. 42: Residuals: $\Xi^{-}K^{*0}$ to ΛK^{+} (0-10% Centrality)

3.1.2 ΛK^- Residuals

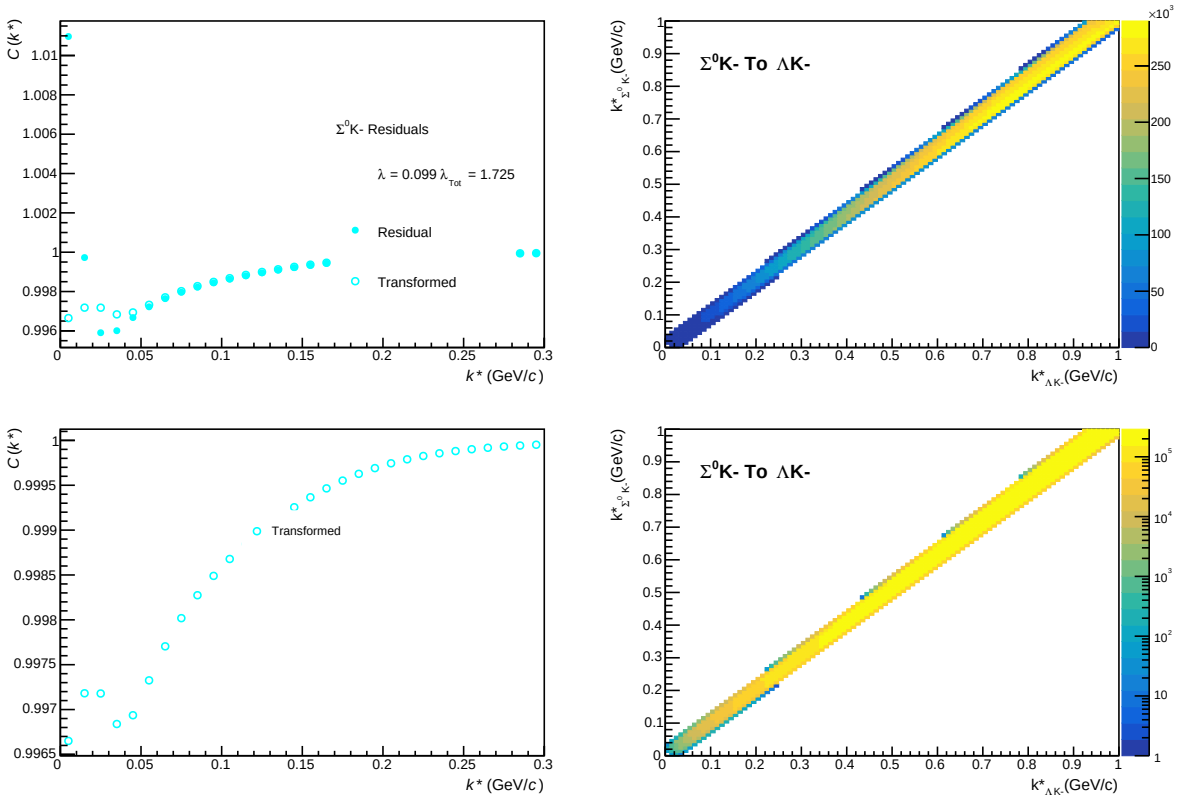

Fig. 43: Residuals: $\Sigma^0 K^-$ to ΛK^- (0-10% Centrality)

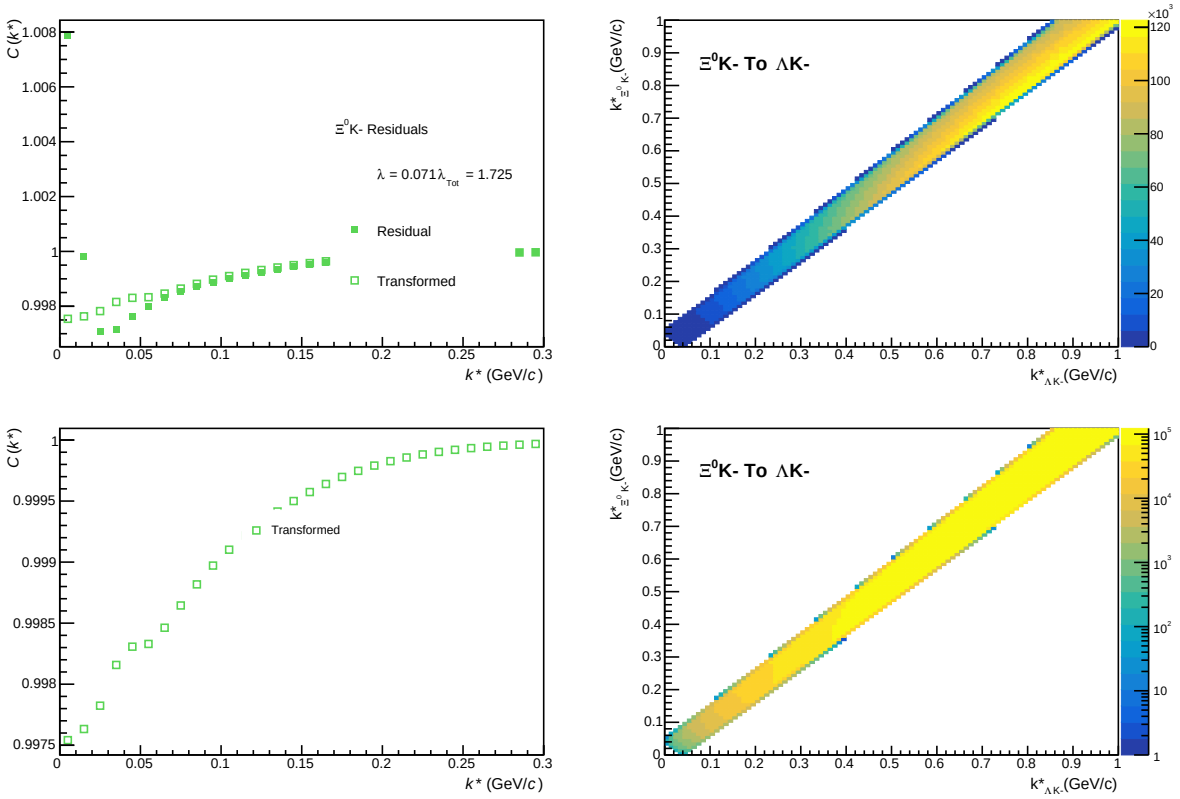

Fig. 44: Residuals: $\Xi^0 K^-$ to ΛK^- (0-10% Centrality)

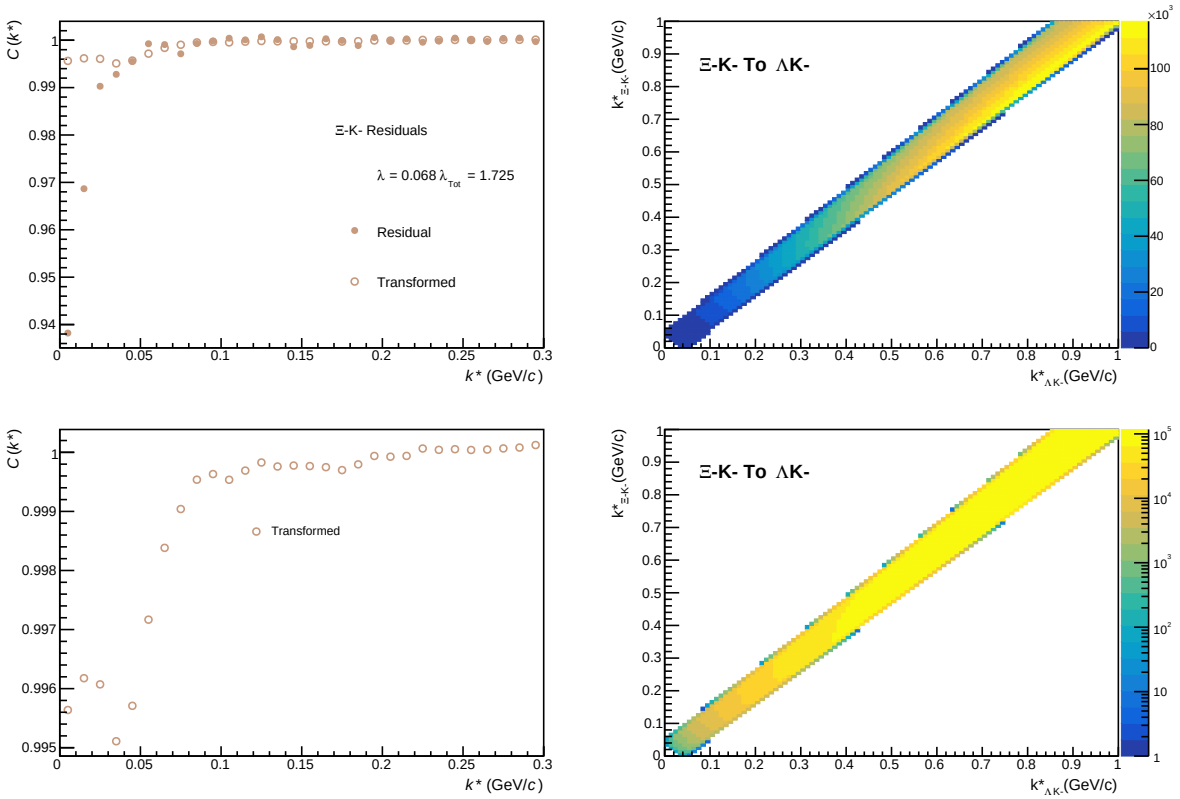

Fig. 45: Residuals: $\Xi^- K^-$ to ΛK^- (0-10% Centrality)

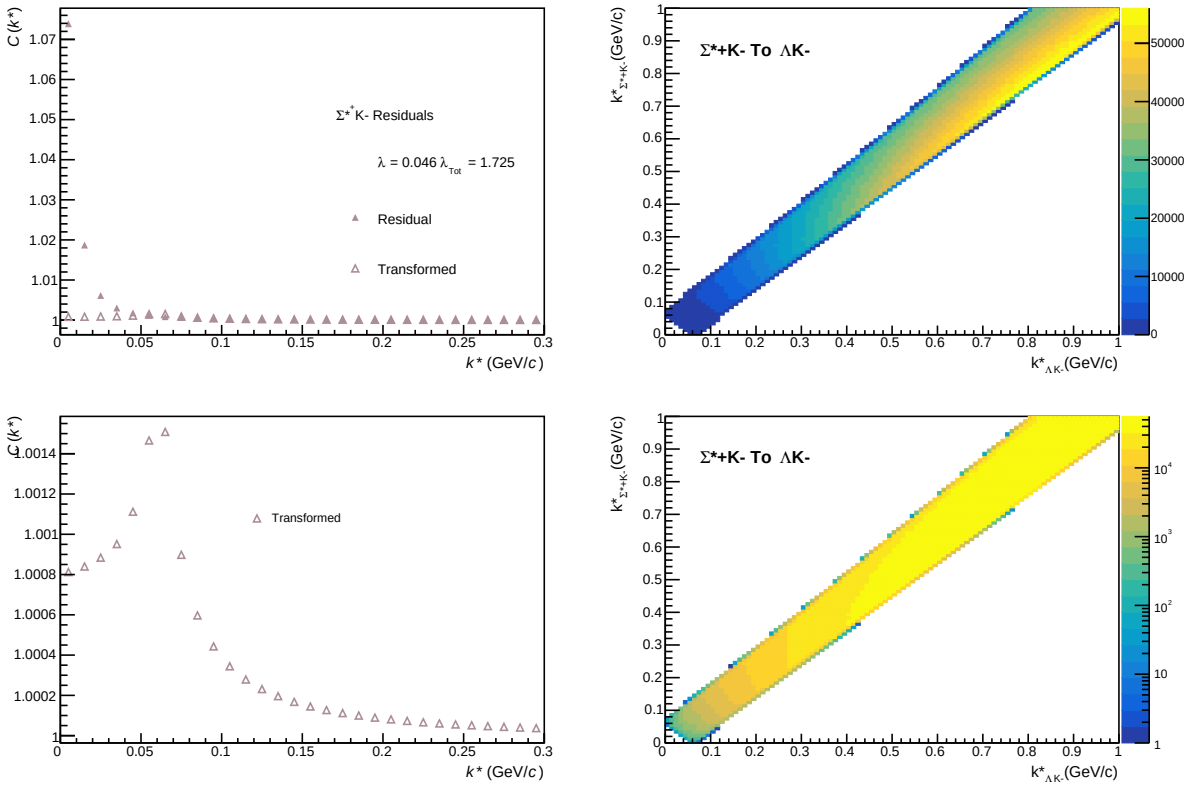

Fig. 46: Residuals: $\Sigma^{*+}K^{-}$ to ΛK^{-} (0-10% Centrality)

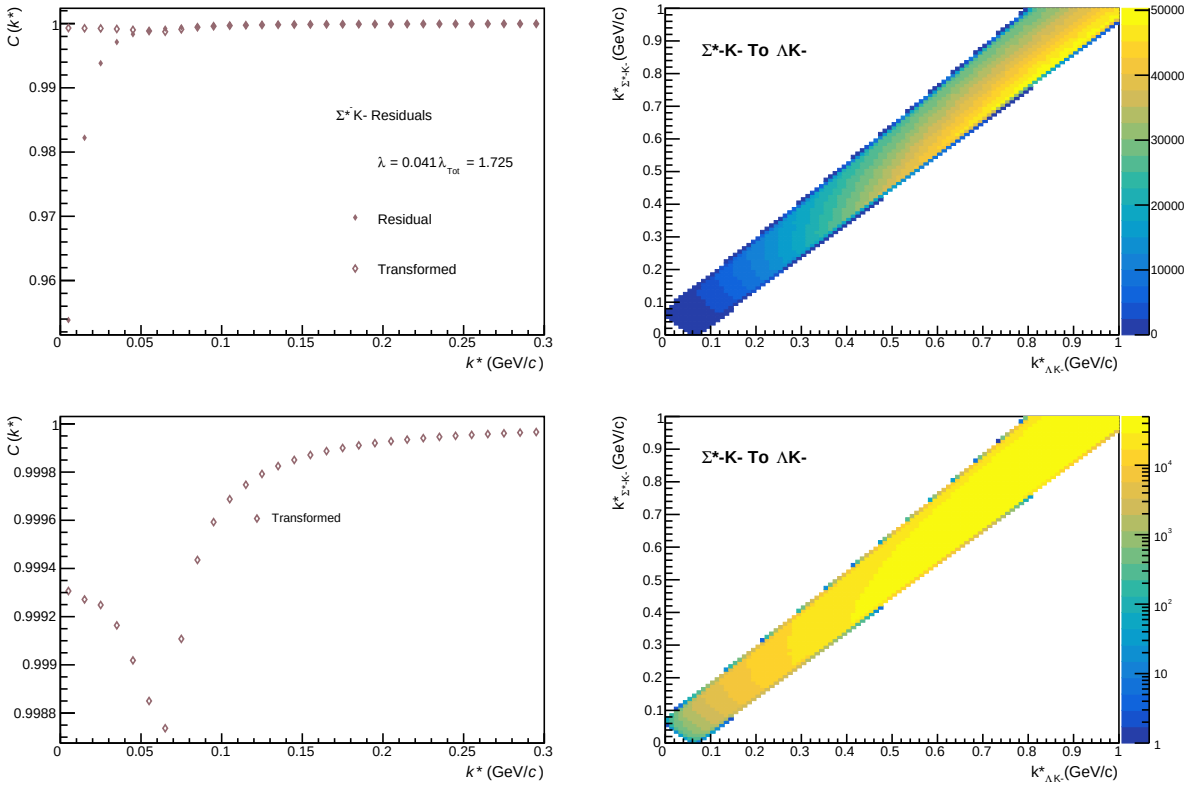

Fig. 47: Residuals: $\Sigma^{*-}K^{-}$ to ΛK^{-} (0-10% Centrality)

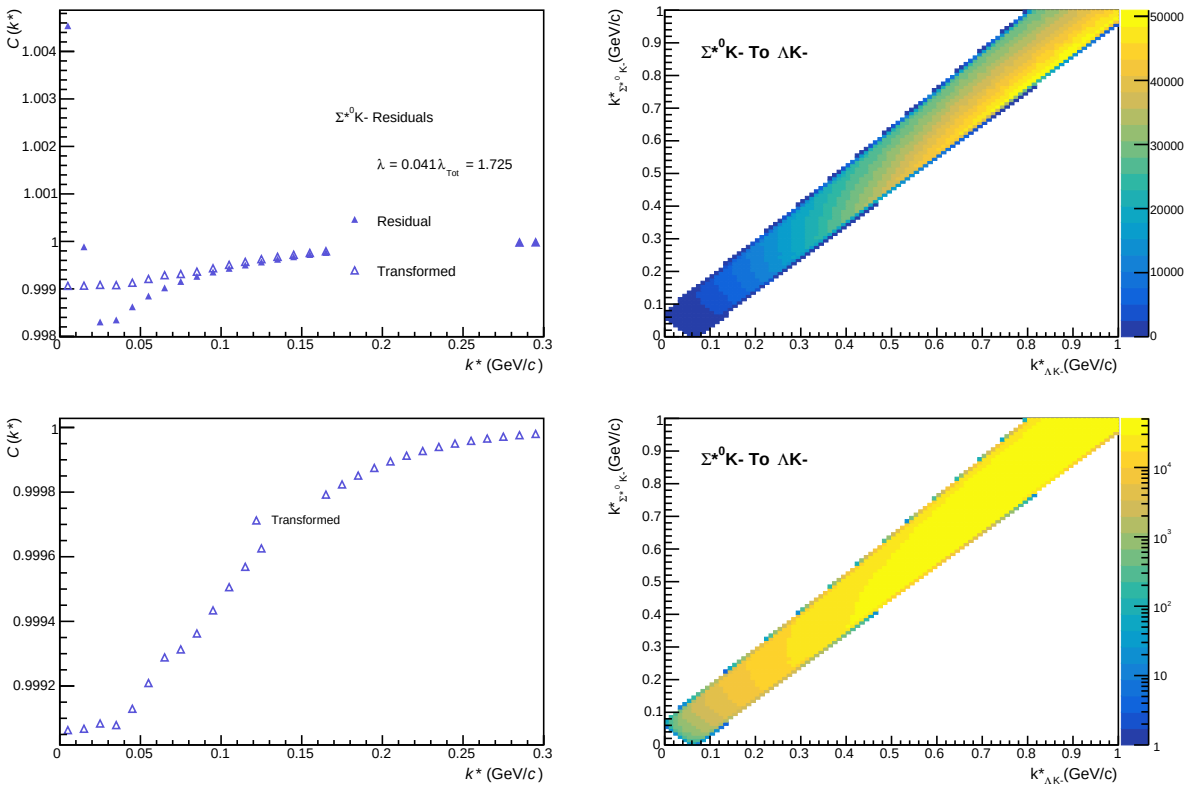

Fig. 48: Residuals: $\Sigma^{*0}K^{-}$ to ΛK^{-} (0-10% Centrality)

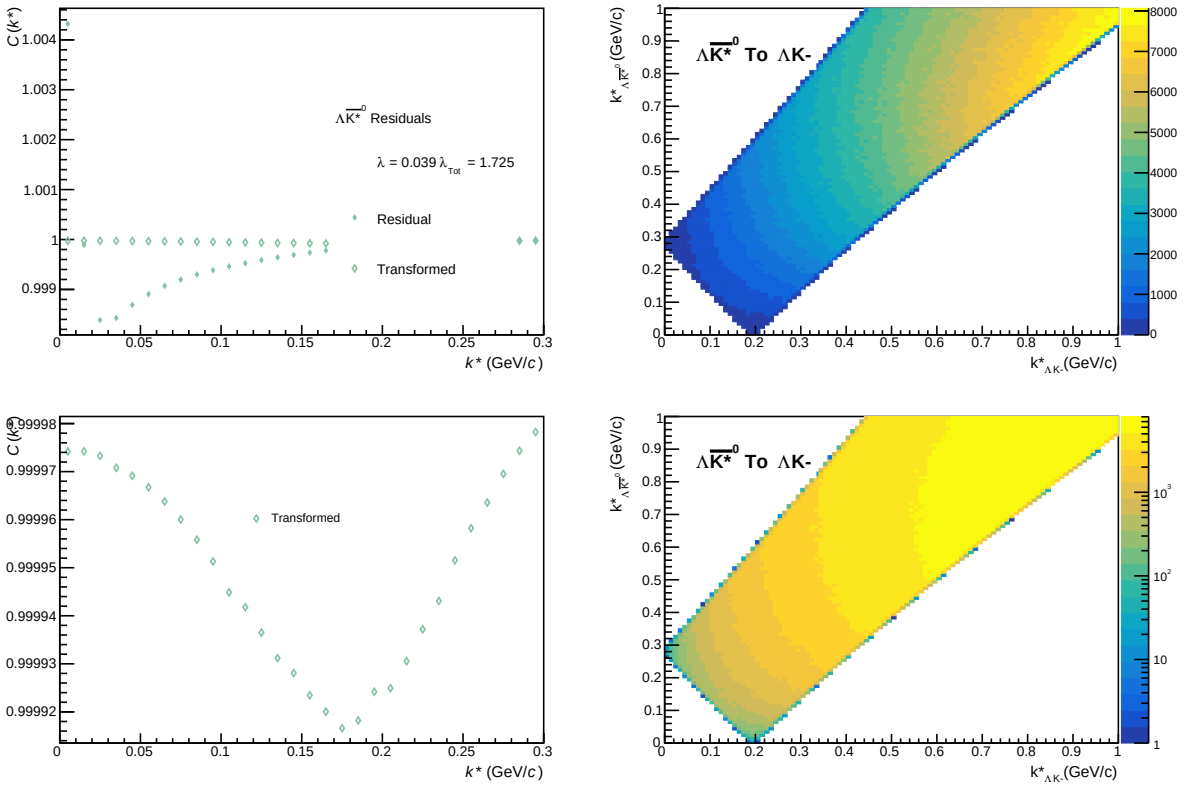

Fig. 49: Residuals: $\Lambda\bar{K}^{*0}$ to ΛK^{-} (0-10% Centrality)

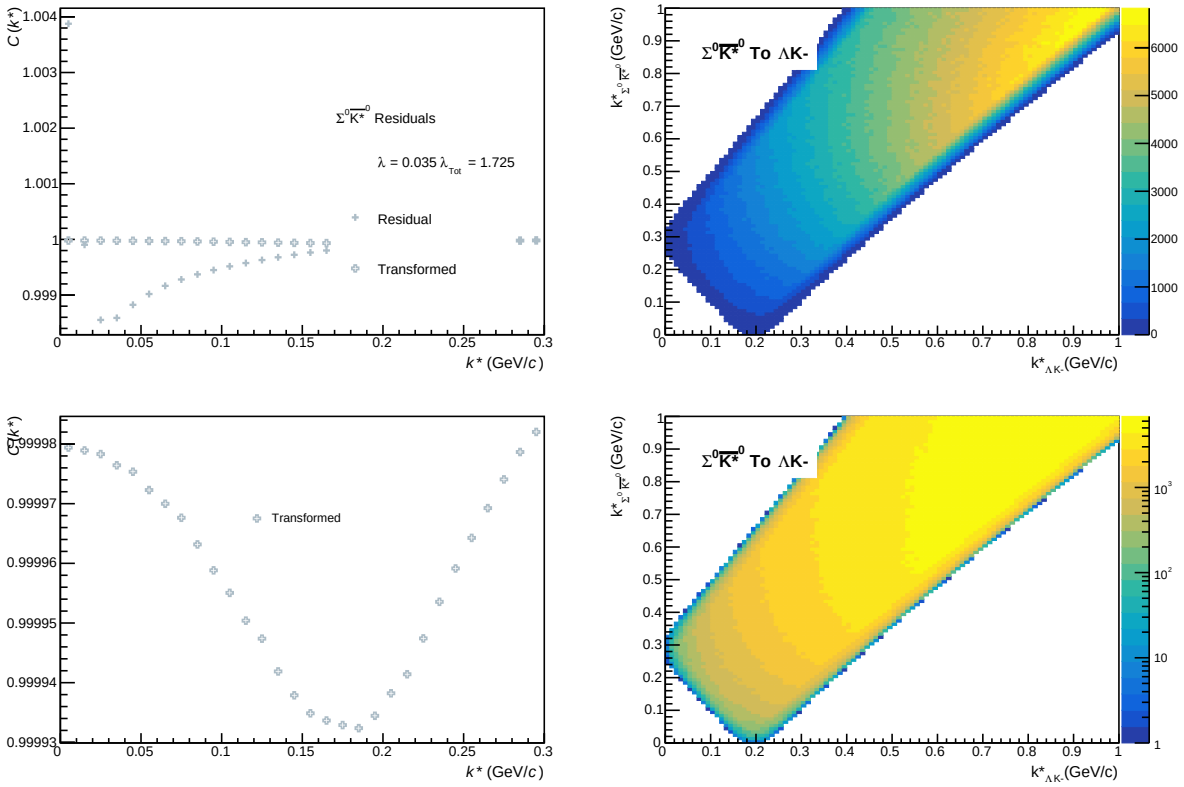

Fig. 50: Residuals: $\Sigma^0\bar{K}^{*0}$ to ΛK^- (0-10% Centrality)

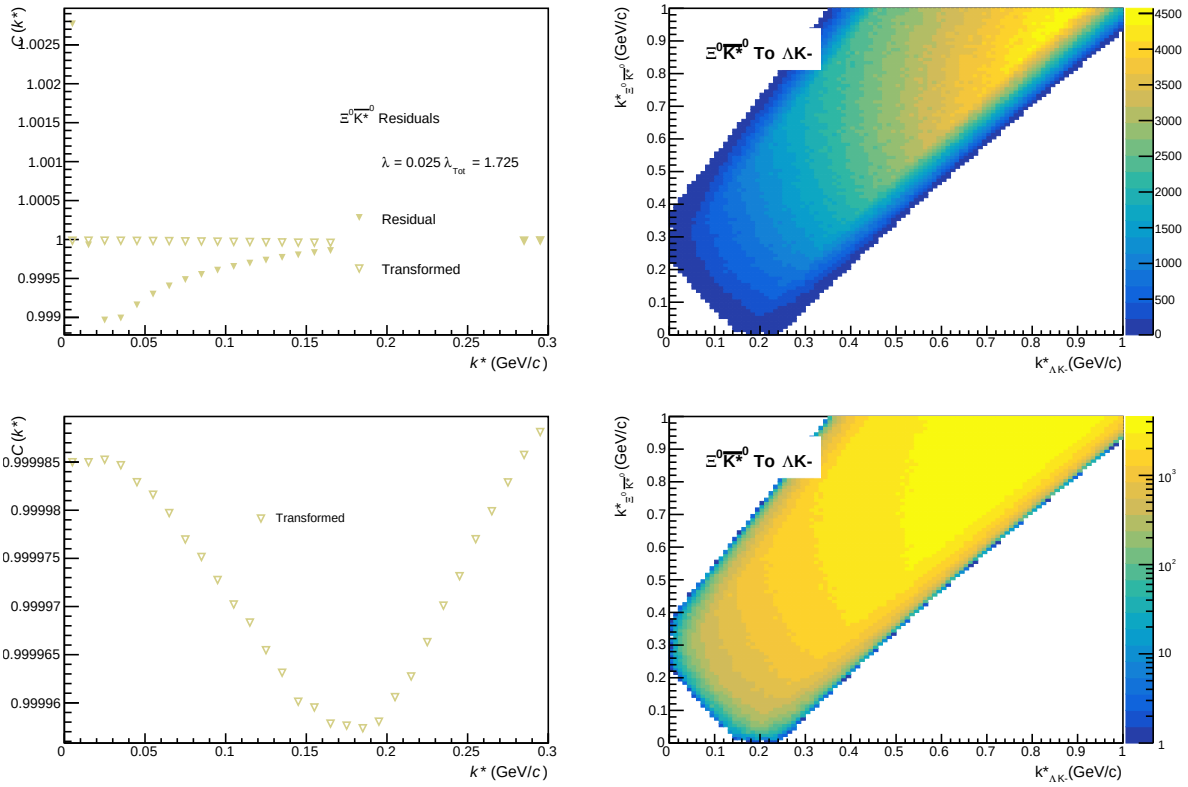

Fig. 51: Residuals: $\Xi^0\bar{K}^{*0}$ to ΛK^- (0-10% Centrality)

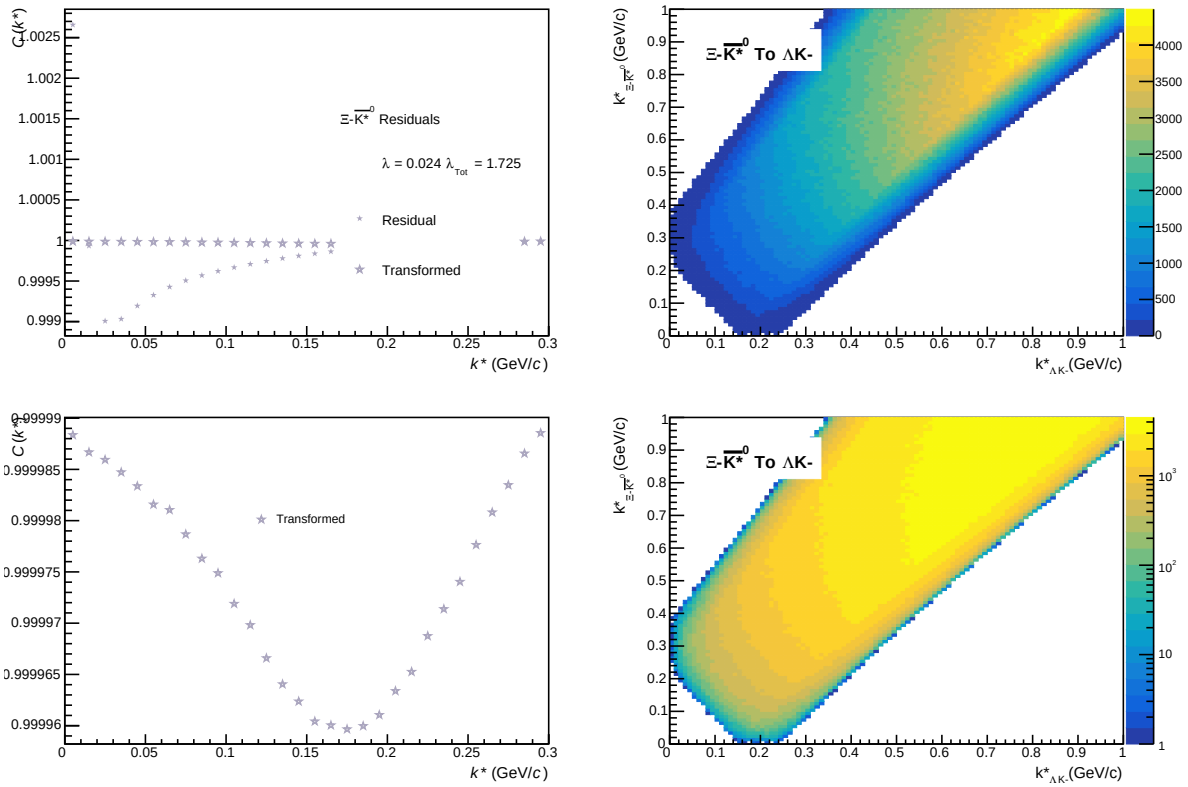

Fig. 52: Residuals: $\Xi^{-}\bar{K}^{*0}$ to ΛK^{-} (0-10% Centrality)

3.1.3 ΛK^0_S *Residuals*

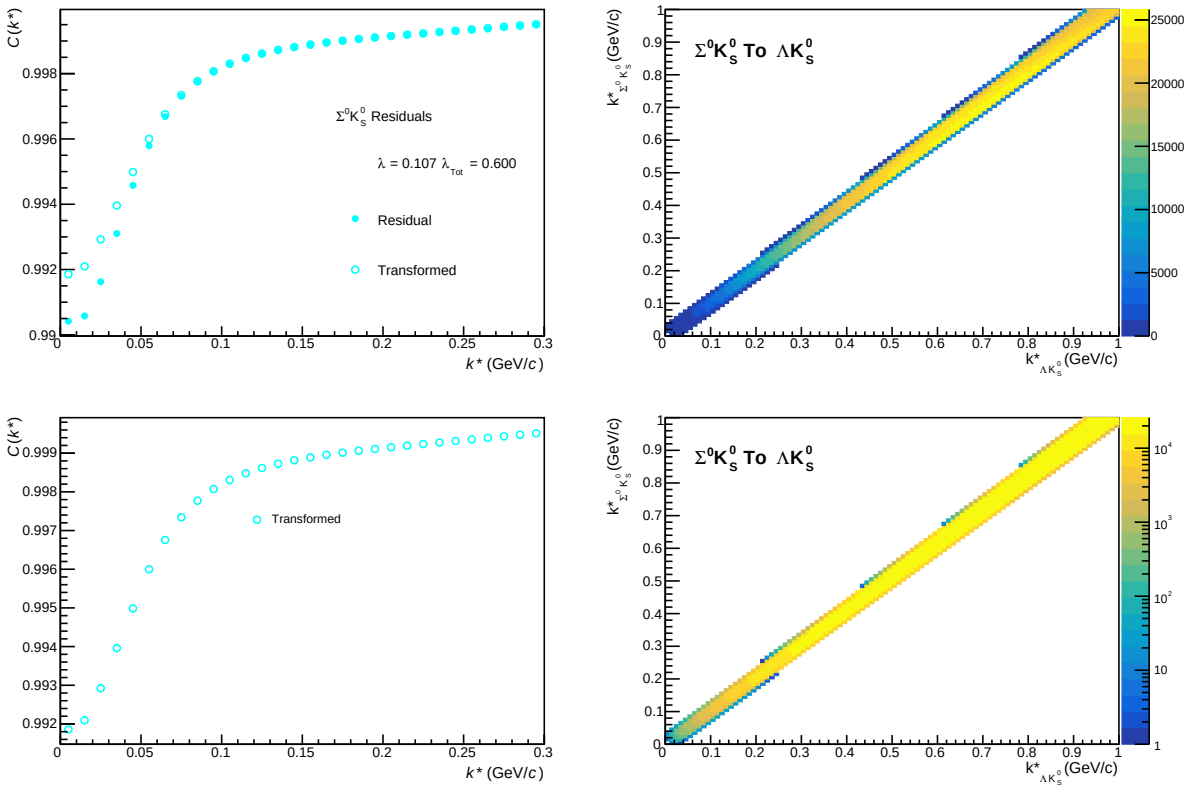

Fig. 53: Residuals: $\Sigma^0 K^0_S$ to ΛK^0_S (0-10% Centrality)

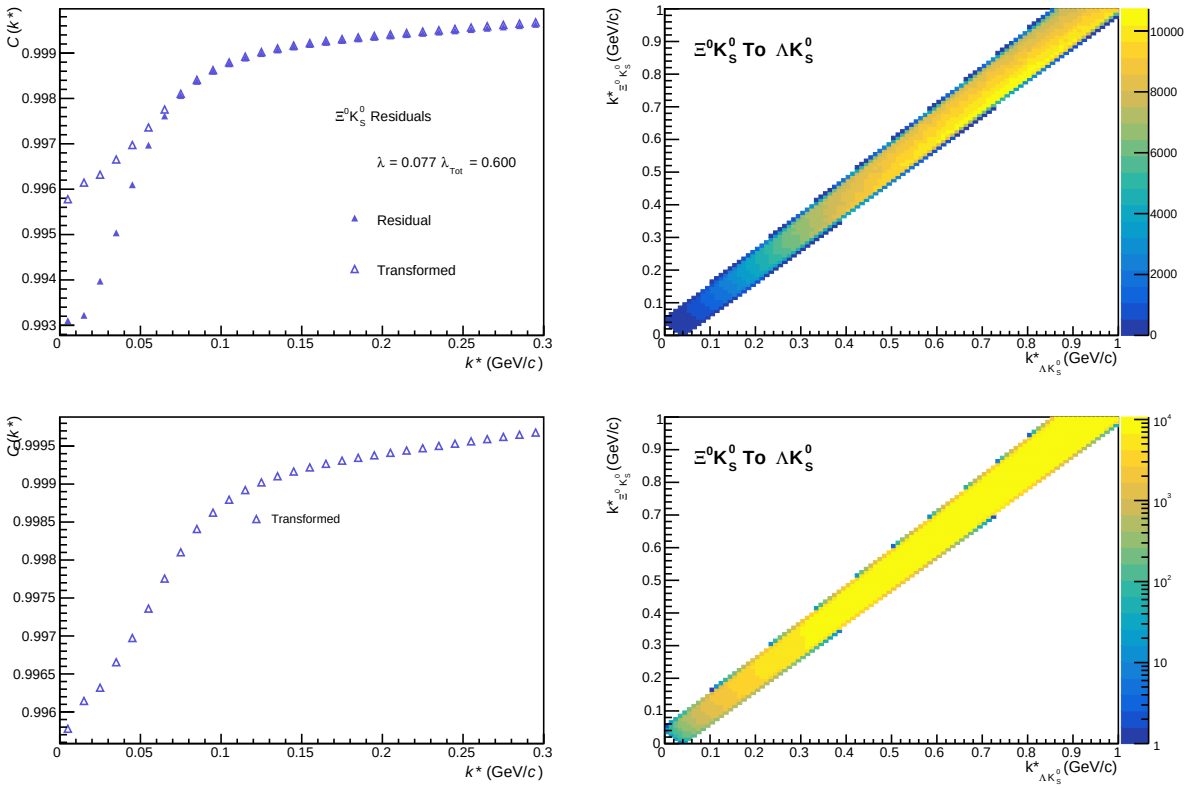

Fig. 54: Residuals: $\Xi^0 K^0_S$ to ΛK^0_S (0-10% Centrality)

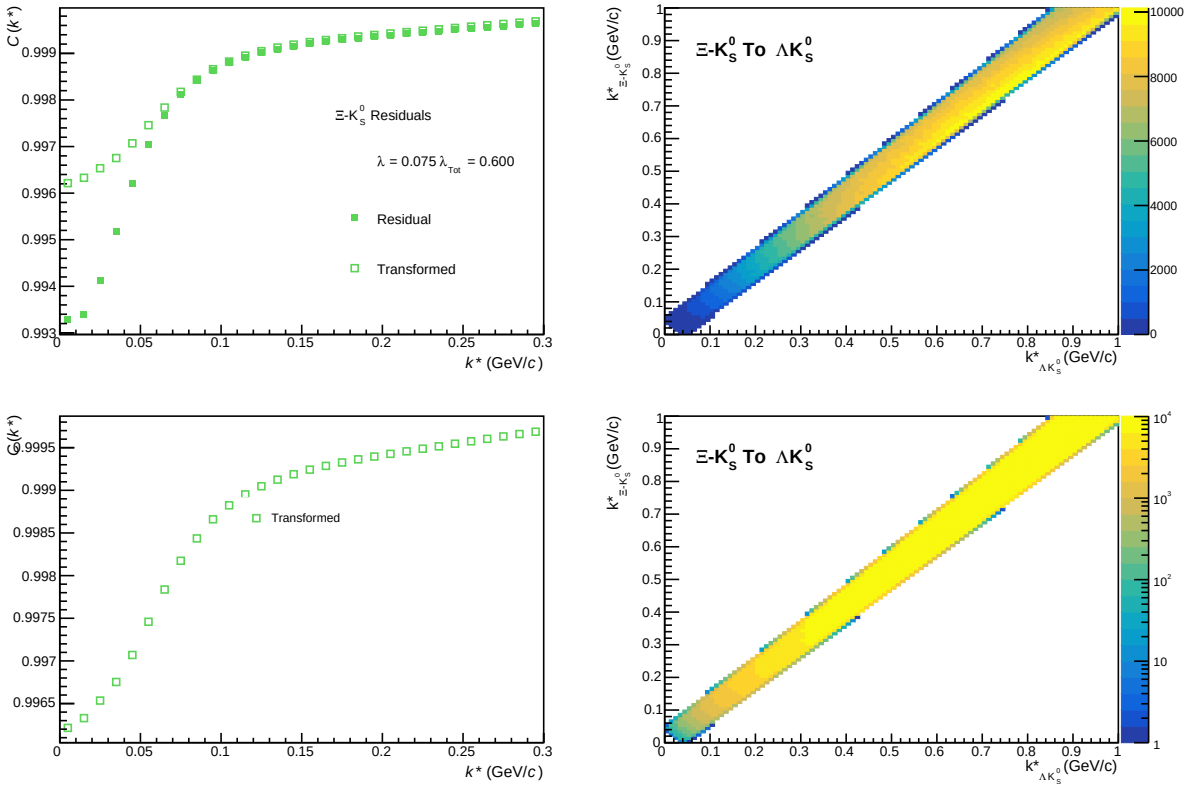

Fig. 55: Residuals: $\Xi^- K^0_S$ to ΛK^0_S (0-10% Centrality)

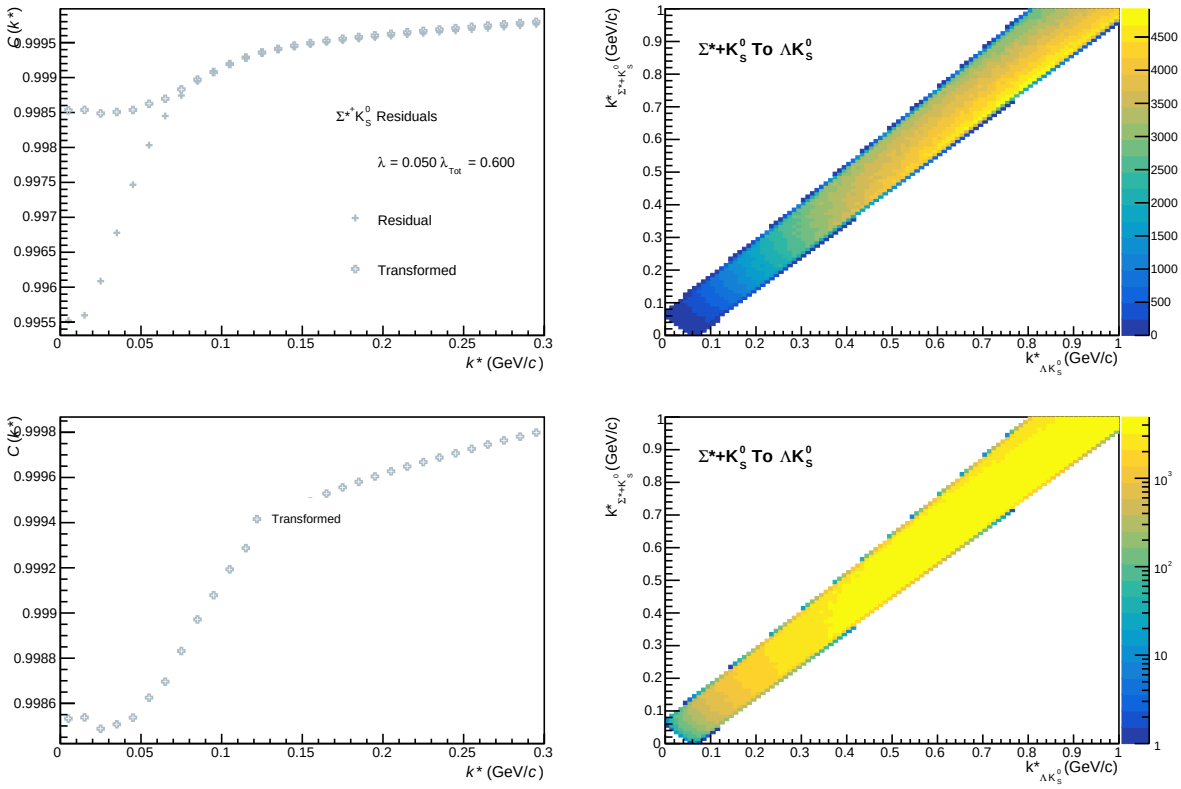

Fig. 56: Residuals: $\Sigma^{*+}K^0_S$ to ΛK^0_S (0-10% Centrality)

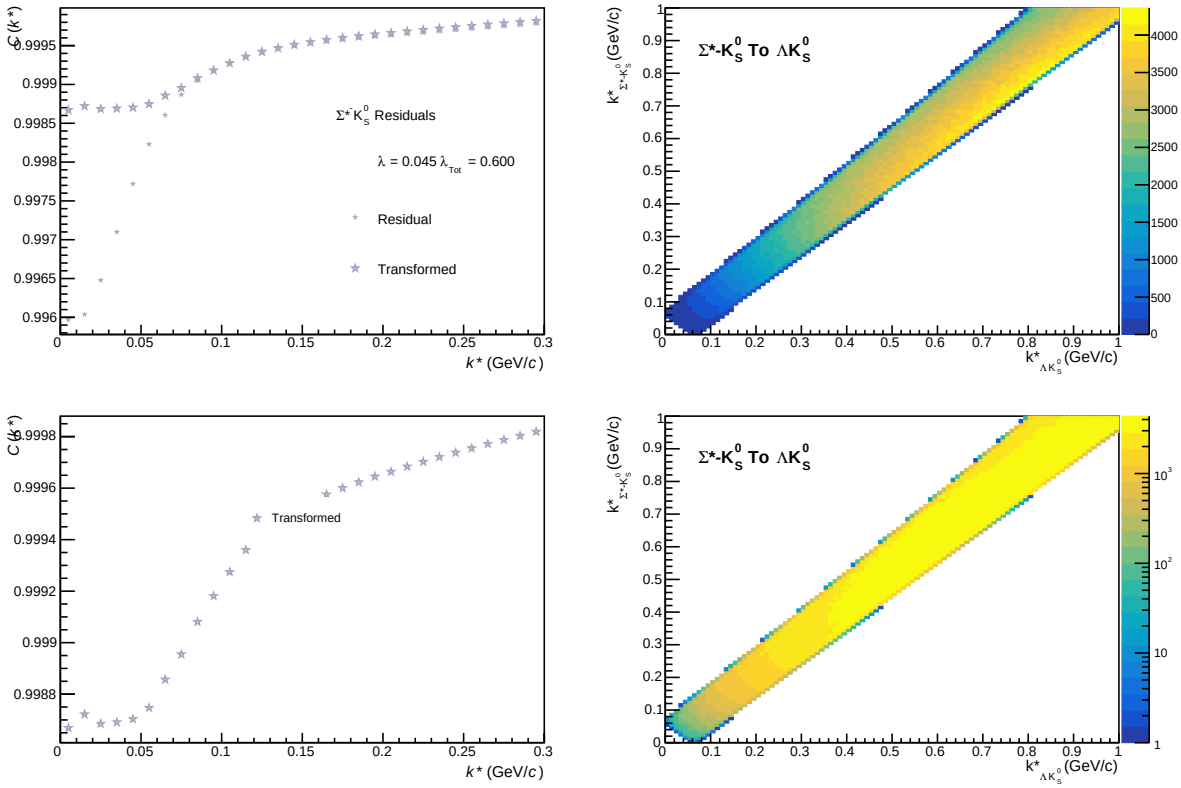

Fig. 57: Residuals: $\Sigma^{*-}K^0_S$ to ΛK^0_S (0-10% Centrality)

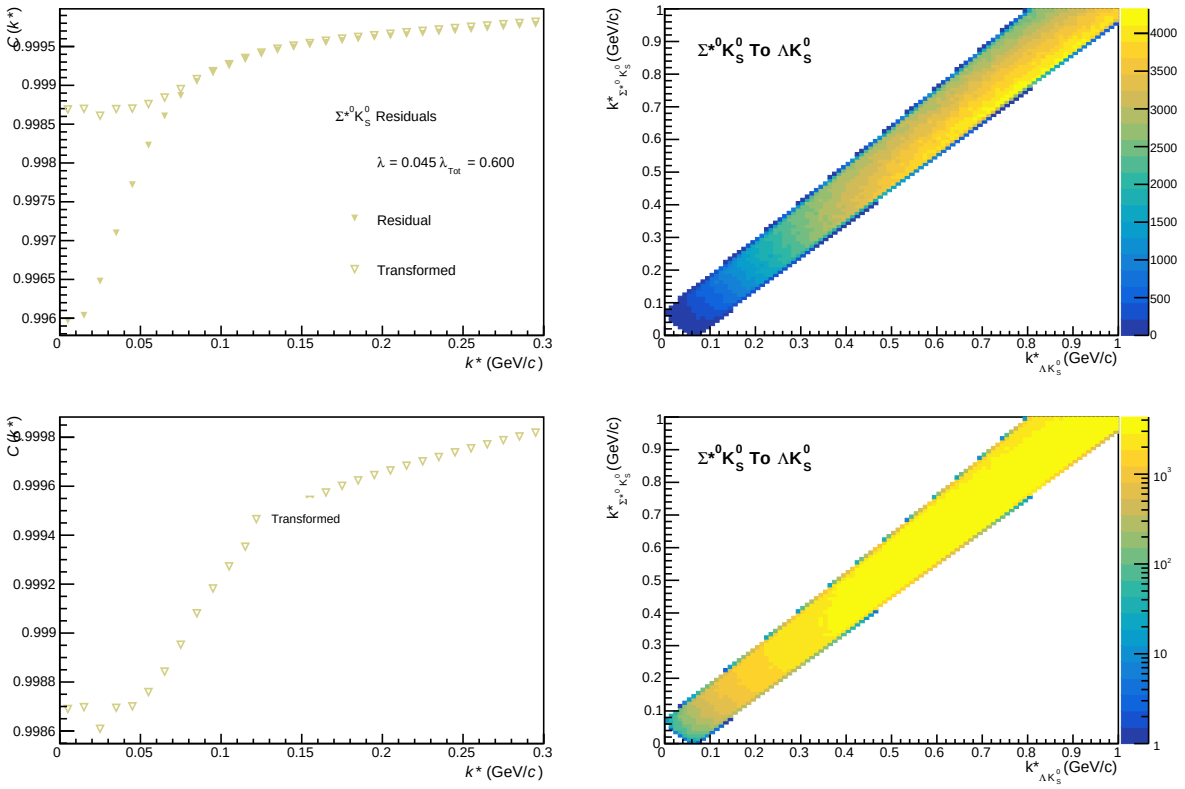

Fig. 58: Residuals: $\Sigma^{*0}K^0_S$ to ΛK^0_S (0-10% Centrality)

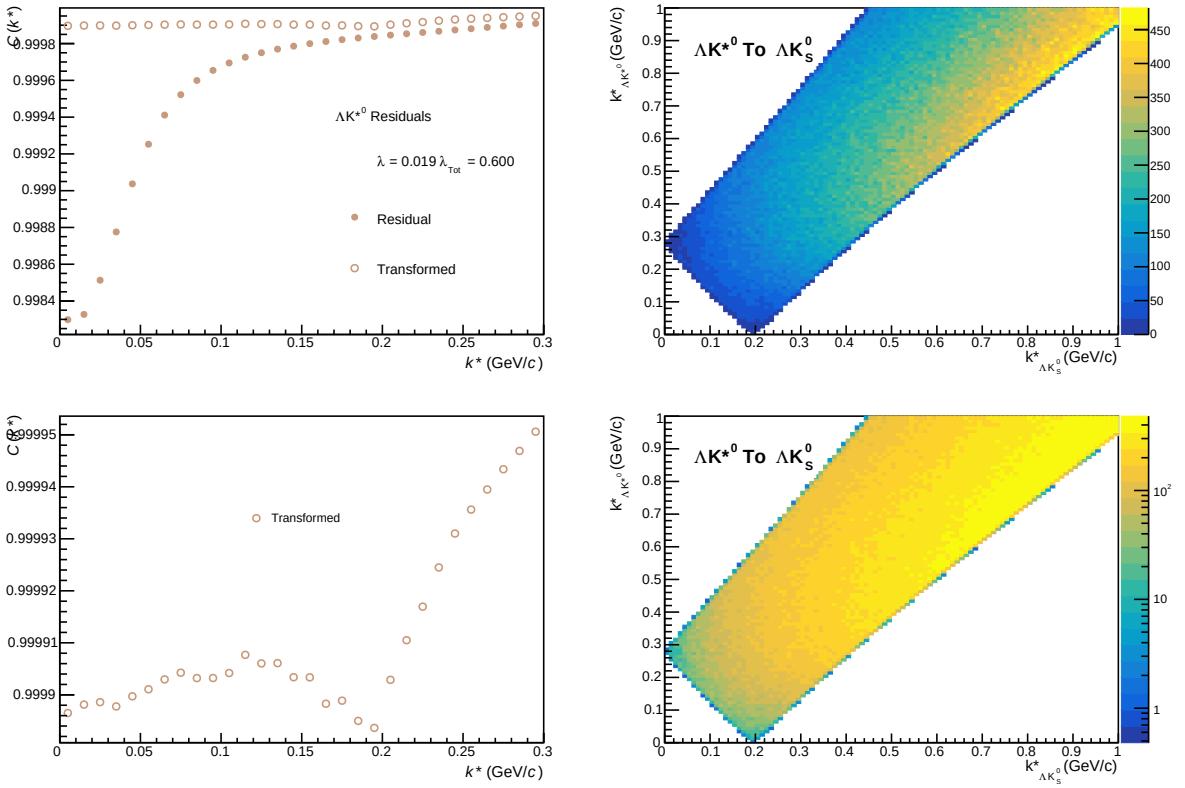

Fig. 59: Residuals: ΛK^{*0} to ΛK^0_S (0-10% Centrality)

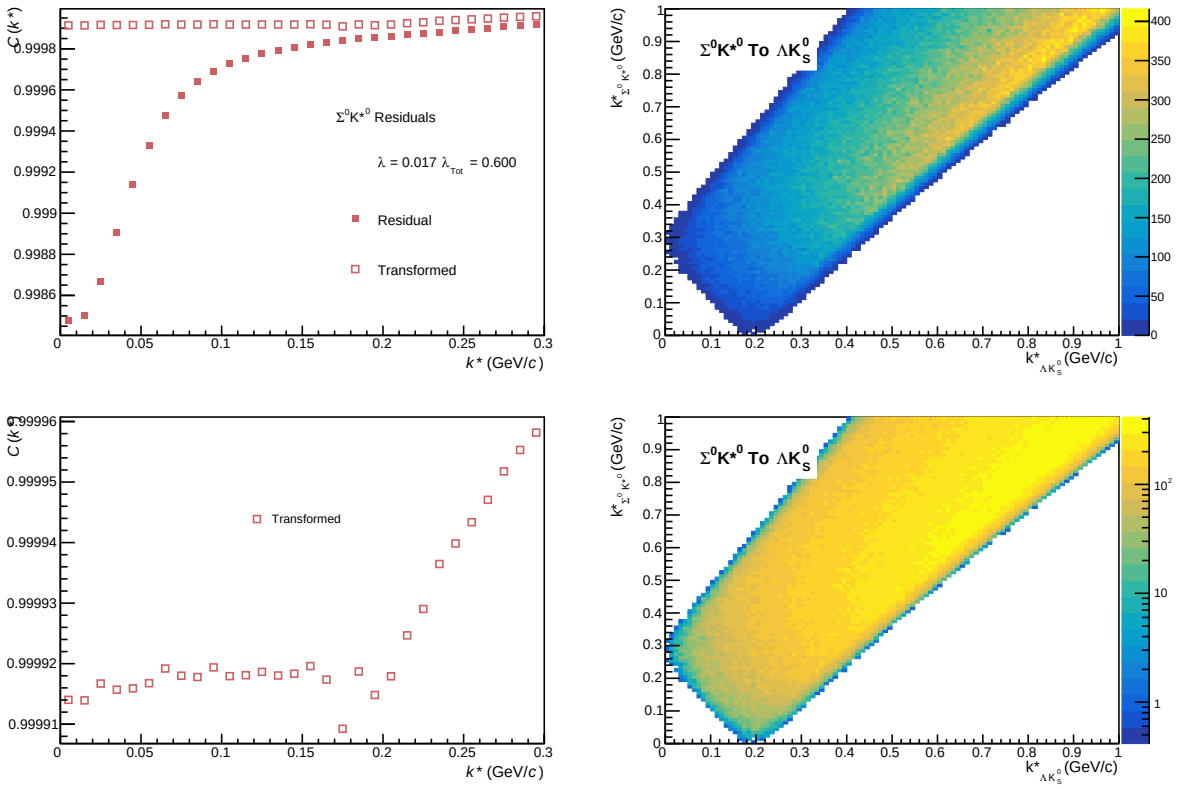

Fig. 60: Residuals: $\Sigma^0 K^{*0}$ to ΛK^0_S (0-10% Centrality)

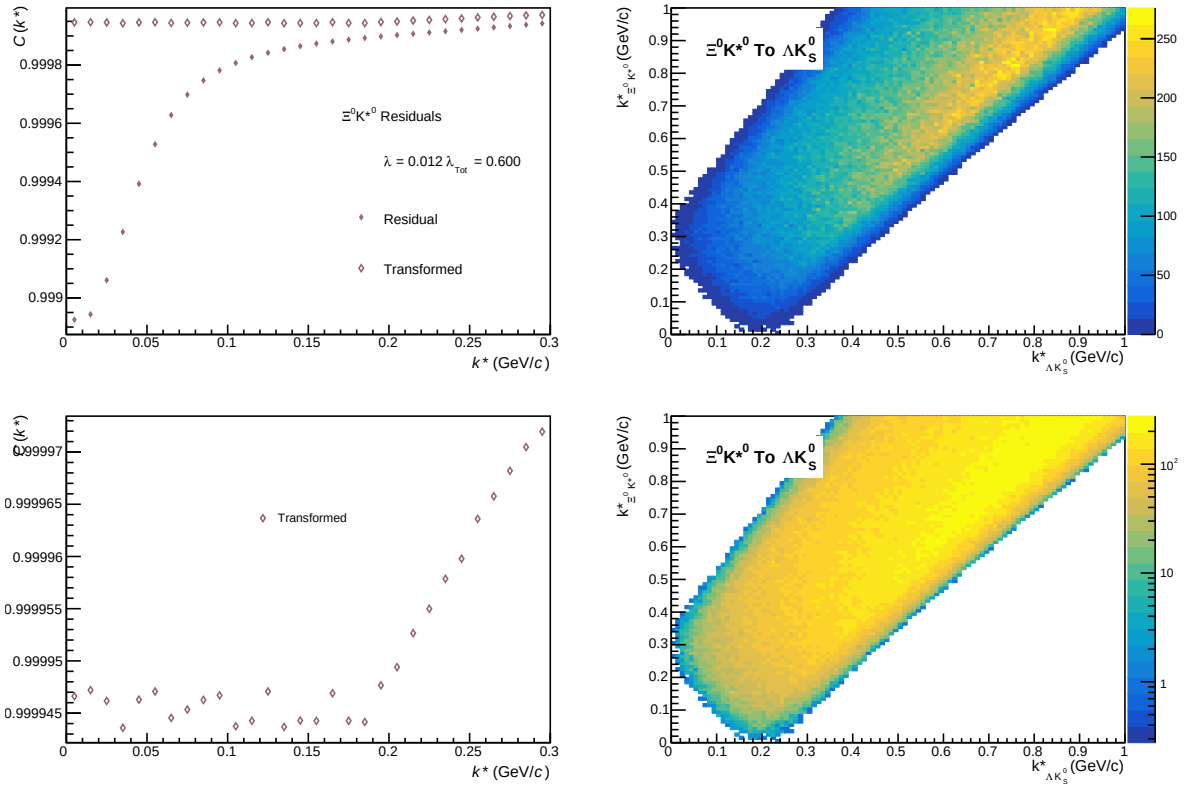

Fig. 61: Residuals: $\Xi^0 K^{*0}$ to ΛK^0_S (0-10% Centrality)

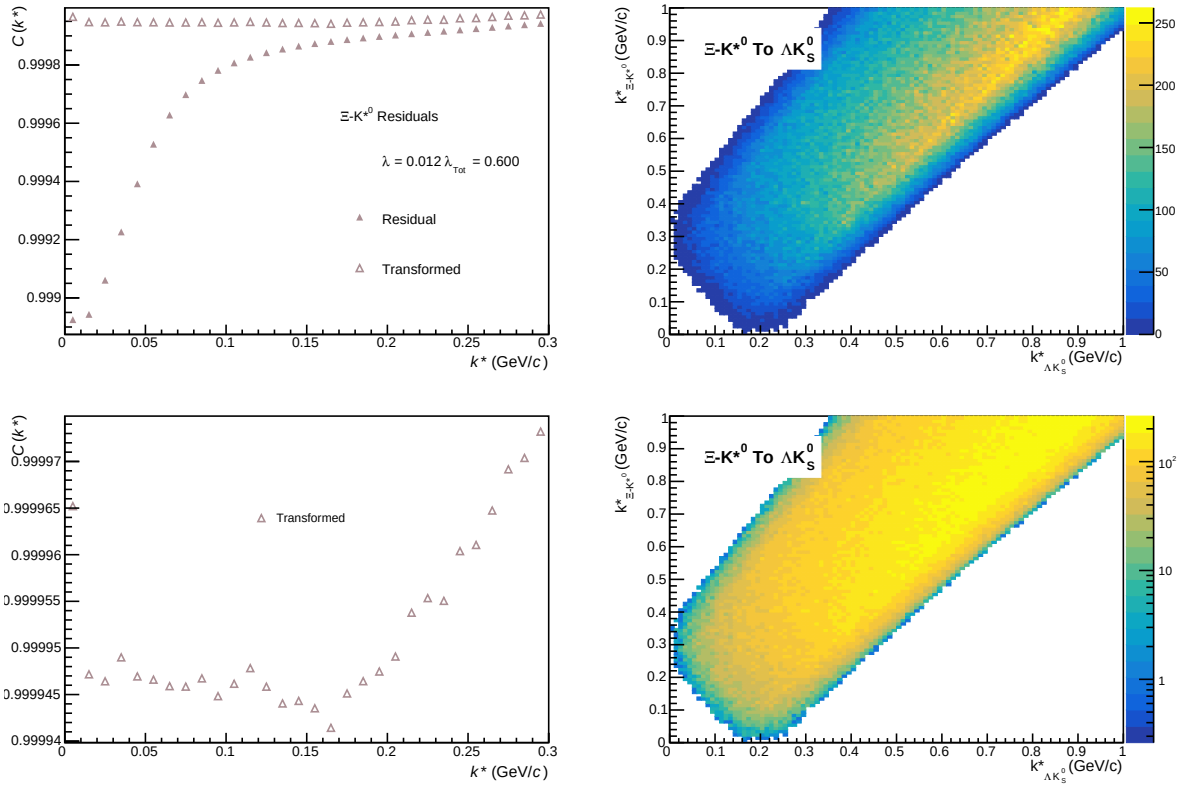

Fig. 62: Residuals: $\Xi^{-}K^{*0}$ to ΛK^{0}_{S} (0-10% Centrality)

4 Useful Gaussian Integrals

4.1 Simple univariate Gaussian integral

$$\begin{aligned} I &= \int_{-\infty}^{\infty} e^{-x^2/2\sigma^2} dx \\ \rightarrow I^2 &= \int_{-\infty}^{\infty} e^{-x^2/2\sigma^2} dx \int_{-\infty}^{\infty} e^{-y^2/2\sigma^2} dy = \int_{-\infty}^{\infty}\int_{-\infty}^{\infty} e^{-(x^2+y^2)/2\sigma^2} dxdy \\ &= \int_0^{\infty}\int_0^{2\pi} e^{-r^2/2\sigma^2} rdrd\theta = -2\pi\sigma^2 \int_0^{\infty} e^{-r^2/2\sigma^2} \frac{-r}{\sigma^2} dr = 2\pi\sigma^2 \\ \Rightarrow I &= \sigma\sqrt{2\pi} \end{aligned} \tag{1}$$

This also implies

$$\int_{-\infty}^{\infty} e^{-(x-\mu)^2/2\sigma^2} dx = \sigma\sqrt{2\pi} \tag{2}$$

This can be shown by making the substitution $x \rightarrow x-\mu$; but, intuitively this makes sense, as the area under a Gaussian curve does not depend on where the curve is located.

4.2 Product of two univariate Gaussian integrals

$$\begin{aligned} f(x) &= \frac{1}{\sigma_f\sqrt{2\pi}} \exp\left[-\frac{(x-\mu_f)^2}{2\sigma_f^2}\right] \\ g(x) &= \frac{1}{\sigma_g\sqrt{2\pi}} \exp\left[-\frac{(x-\mu_g)^2}{2\sigma_g^2}\right] \\ \Rightarrow f(x)g(x) &= \frac{1}{2\pi\sigma_f\sigma_g} \exp\left[-\frac{(x-\mu_f)^2}{2\sigma_f^2} - \frac{(x-\mu_g)^2}{2\sigma_g^2}\right] \\ &\equiv \frac{1}{2\pi\sigma_f\sigma_g} \exp[-\beta] \end{aligned} \tag{3}$$

$$\begin{aligned} \beta &= \frac{(x-\mu_f)^2}{2\sigma_f^2} + \frac{(x-\mu_g)^2}{2\sigma_g^2} \\ &= \frac{2\sigma_g^2[x^2-2\mu_f x+\mu_f^2] + 2\sigma_f^2[x^2-2\mu_g x+\mu_g^2]}{4\sigma_f^2\sigma_g^2} \\ &= \frac{(\sigma_f^2+\sigma_g^2)x^2 - 2(\mu_f\sigma_g^2+\mu_g\sigma_f^2)x + \mu_f^2\sigma_g^2+\mu_g\sigma_f^2}{2\sigma_f^2\sigma_g^2} \\ &= \frac{x^2 - 2\frac{\mu_f\sigma_g^2+\mu_g\sigma_f^2}{\sigma_f^2+\sigma_g^2}x + \frac{\mu_f^2\sigma_g^2+\mu_g^2\sigma_f^2}{\sigma_f^2+\sigma_g^2}}{2\frac{\sigma_f^2\sigma_g^2}{\sigma_f^2+\sigma_g^2}} \end{aligned} \tag{4}$$

$$\text{Define : } \alpha \equiv \frac{\mu_f\sigma_g^2+\mu_g\sigma_f^2}{\sigma_f^2+\sigma_g^2}$$

$$\Rightarrow \beta = \frac{(x^2-2\alpha x+\alpha^2) - \alpha^2 + \frac{\mu_f^2\sigma_g^2+\mu_g^2\sigma_f^2}{\sigma_f^2+\sigma_g^2}}{2\frac{\sigma_f^2\sigma_g^2}{\sigma_f^2+\sigma_g^2}}$$

$$\begin{aligned}
\frac{\mu_f^2\sigma_g^2+\mu_g^2\sigma_f^2}{\sigma_f^2+\sigma_g^2}-\alpha^2 &= \frac{\mu_f^2\sigma_g^2+\mu_g^2\sigma_f^2}{\sigma_f^2+\sigma_g^2}-\left(\frac{\mu_f\sigma_g^2+\mu_g\sigma_f^2}{\sigma_f^2+\sigma_g^2}\right)^2 \\
&= \frac{1}{(\sigma_f^2+\sigma_g^2)^2}\left[(\mu_f^2\sigma_g^2+\mu_g^2\sigma_f^2)(\sigma_f^2+\sigma_g^2)-(\mu_f\sigma_g^2+\mu_g\sigma_f^2)^2\right] \\
&= \frac{1}{(\sigma_f^2+\sigma_g^2)^2}\left[\mu_f^2\sigma_f^2\sigma_g^2+\mu_g^2\sigma_f^2\sigma_g^2+\mu_f^2\sigma_g^4+\mu_g^2\sigma_f^4-\ldots\right. \\
&\qquad \left.-\mu_f^2\sigma_g^4-\mu_g^2\sigma_f^4-2\mu_f\mu_g\sigma_f^2\sigma_g^2\right] \\
&= \frac{\sigma_f^2\sigma_g^2}{(\sigma_f^2+\sigma_g^2)^2}\left[\mu_f^2-2\mu_f\mu_g+\mu_g^2\right] \\
&= \frac{\sigma_f^2\sigma_g^2}{(\sigma_f^2+\sigma_g^2)^2}(\mu_f-\mu_g)^2
\end{aligned} \tag{5}$$

$$\begin{aligned}
\beta &= \frac{(x^2-2\alpha x+\alpha^2)-\alpha^2+\frac{\mu_f^2\sigma_g^2+\mu_g^2\sigma_f^2}{\sigma_f^2+\sigma_g^2}}{2\frac{\sigma_f^2\sigma_g^2}{\sigma_f^2+\sigma_g^2}} \\
&= \frac{(x-\alpha)^2+\frac{\sigma_f^2\sigma_g^2}{(\sigma_f^2+\sigma_g^2)^2}(\mu_f-\mu_g)^2}{2\frac{\sigma_f^2\sigma_g^2}{\sigma_f^2+\sigma_g^2}} \\
\text{Define : } \gamma^2 &= \frac{\sigma_f^2\sigma_g^2}{\sigma_f^2+\sigma_g^2} \\
\beta &= \frac{(x-\alpha)^2}{2\gamma^2}+\frac{(\mu_f-\mu_g)^2}{2(\sigma_f^2+\sigma_g^2)}
\end{aligned} \tag{6}$$

$$\begin{aligned}
f(x)g(x) &= \frac{1}{2\pi\sigma_f\sigma_g}e^{-\beta} = \frac{1}{2\pi\sigma_f\sigma_g}\exp\left[-\frac{(x-\alpha)^2}{2\gamma^2}\right]\exp\left[\frac{(\mu_f-\mu_g)^2}{2(\sigma_f^2+\sigma_g^2)}\right] \\
&= \frac{1}{\sigma_f\sigma_g}\gamma\sqrt{(\sigma_f^2+\sigma_g^2)}\times\frac{1}{\gamma\sqrt{2\pi}}\exp\left[-\frac{(x-\alpha)^2}{2\gamma^2}\right]\times\ldots \\
&\quad\times\frac{1}{\sqrt{(\sigma_f^2+\sigma_g^2)}\sqrt{2\pi}}\exp\left[\frac{(\mu_f-\mu_g)^2}{2(\sigma_f^2+\sigma_g^2)}\right] \\
\Rightarrow f(x)g(x) &= \frac{1}{\gamma\sqrt{2\pi}}\exp\left[-\frac{(x-\alpha)^2}{2\gamma^2}\right]S_{fg} \\
S_{fg} &= \frac{\gamma\sqrt{(\sigma_f^2+\sigma_g^2)}}{\sigma_f\sigma_g}\frac{1}{\sqrt{(\sigma_f^2+\sigma_g^2)}\sqrt{2\pi}}\exp\left[-\frac{(\mu_f-\mu_g)^2}{2(\sigma_f^2+\sigma_g^2)}\right] \\
&= \frac{1}{\sqrt{2\pi(\sigma_f^2+\sigma_g^2)}}\exp\left[-\frac{(\mu_f-\mu_g)^2}{2(\sigma_f^2+\sigma_g^2)}\right]
\end{aligned} \tag{7}$$

$$\begin{aligned}\int_{-\infty}^{\infty} f(x)g(x)dx &= \frac{S_{fg}}{\gamma\sqrt{2\pi}}\int_{-\infty}^{\infty}\exp\left[-\frac{(x-\alpha)^2}{2\gamma^2}\right] = S_{fg} \\ &= \frac{1}{\sqrt{2\pi(\sigma_f^2+\sigma_g^2)}}\exp\left[-\frac{(\mu_f-\mu_g)^2}{2(\sigma_f^2+\sigma_g^2)}\right]\end{aligned} \tag{8}$$

4.3 Univariate Gaussian with linear term in exponential

$$I = \int_{-\infty}^{\infty}\exp\left[-\frac{x^2}{2\sigma^2}+Jx\right] \tag{9}$$

Just as above, the idea is to complete the square

$$\begin{aligned}\frac{x^2}{2\sigma^2} - Jx &= \frac{1}{2\sigma^2}\left[x^2 - 2\sigma^2 Jx + (\sigma^2 J)^2 - (\sigma^2 J)^2\right] \\ &= \frac{1}{2\sigma^2}\left(x-\sigma^2 J\right)^2 - \frac{1}{2\sigma^2}(\sigma^2 J)^2 = \frac{\left(x-\sigma^2 J\right)^2}{2\sigma^2} - \frac{(\sigma J)^2}{2}\end{aligned} \tag{10}$$

Therefore, I find:

$$\begin{aligned}I &= \int_{-\infty}^{\infty}\exp\left[-\frac{x^2}{2\sigma^2}+Jx\right] = \int_{-\infty}^{\infty}\exp\left[\frac{\left(x-\sigma^2 J\right)^2}{2\sigma^2} - \frac{(\sigma J)^2}{2}\right] \\ &= \sigma\sqrt{2\pi}\exp\left[\frac{(\sigma J)^2}{2}\right]\end{aligned} \tag{11}$$